Molecular Therapy
Original Article

miR24-2 Promotes Malignant Progression of Human Liver Cancer Stem Cells by Enhancing Tyrosine Kinase Src Epigenetically

Liyan Wang,[1,3] Xiaonan Li,[1,3] Wei Zhang,[1,3] Yuxin Yang,[1] Qiuyu Meng,[1] Chen Wang,[1] Xiaoru Xin,[1] Xiaoxue Jiang,[1] Shuting Song,[1] Yanan Lu,[1] Hu Pu,[1] Xin Gui,[1] Tianming Li,[1] Jie Xu,[2] Jiao Li,[2] Song Jia,[2] and Dongdong Lu[1]

[1]Shanghai Putuo District People's Hospital, School of Life Science and Technology, Tongji University, Shanghai 200092, China; [2]School of Medicine, Tongji University, Shanghai 200092, China

MicroRNA24-2 (miR24-2) is associated with human tumorigenesis; however, its molecular mechanisms are poorly understood. Herein, our findings demonstrate that miR24-2 promotes the proliferation ability *in vitro* and the tumorigenic ability *in vivo* in human liver cancer stem cells (hLCSCs). Mechanically, the miR24-2 targets for 3′ UTR (2,627–2,648) of protein arginine methyltransferase 7 (PRMT7) inhibit the translational ability of *prmt7* gene. Moreover, miR24-2 inhibits the di-/tri-methylation of histone H4 arginine 3 by reducing PRMT7 and then promotes the expression of Nanog via long noncoding RNA HULC. Notably, miR24-2 inhibits histone deacetylase HDAC3 through miR675, which promotes the acetylation of histone H4 at lysine 16. Subsequently, miR24-2 enhances the interaction between LC3 and ATG4 dependent on PI3K and triggers cellular autophagy. Strikingly, miR24-2 inhibits the degradation of pyruvate kinase M1 via autophagosome-P62 in hLCSCs. Furthermore, miR24-2 enhances the activity of Src by promoting the binding of PKM1 to the *Src* promoter regions in hLCSCs. In particular, our results also indicate that *src* gene determines the oncogenic functions of miR24-2. These results provided a valuable theoretical basis for the discovery of liver cancer therapeutic targets and diagnosis markers based on miR24-2.

INTRODUCTION

It has been found that human stem cells can be differentiated into malignant stem cells in an unfavorable microenvironment.[1,2] Although most studies currently support malignant tumors that originate from malignant transformation of stem cells, there is still controversy about the mechanism of stem cell deterioration.[3,4] At present, extensive research has been conducted on the mechanism of driving stem cell deterioration; for example, METTL3-eIF3h-mediated mRNA circulation promotes stem cell deterioration, etc.[5] Studies indicate that liver cancer stem cell proliferation and differentiation are deregulated in hepatocarcinogenesis.[6,7] Therefore, targeting liver cancer stem cells may bring hope to curing hepatocellular carcinoma.[8]. So far, it is not clear at any time what causes the accumulation of liver stem cell genetic errors, chromatin programming, and chromosomal instability, and eventually evolves into malignant liver cancer stem cells.

MicroRNA24-2 (miR24-2) is expressed in various tissues of the human body and participates in various physiological processes, e.g., erythropoiesis,[9] lipogenesis,[10] T cell senescence,[11] osteoblast differentiation,[12] cell growth and proliferation, [13–15] cancer cell invasion, and hepatic metastasis.[16] Notably, miR24-2-5p can silence expression of several important genes by targeting the protein arginine methyltransferase 7 (PRMT7).[17] Another study showed that inhibition of miR24-2 significantly altered embryonic stem cell (ESC) differentiation.[18] However, the functions of miR24-2 on liver cancer stem cells are still unclear.

Furthermore, cell proliferation can be altered in response to cellular stress or oncogenic signaling by regulating miR675.[19] And HULC is highly upregulated in hepatocellular carcinoma and is a driver of tumor proliferation, migration, and invasion.[20,21] It is worth mentioning that PRMT7 can regulate the histone methylation modification, especially H4R3me2 and H3K4me3.[22,23] Therefore, it is worthwhile to study how miR24-2 works through miR675, HULC, and PRMT7 in human liver cancer stem cells (hLCSCs).

In this study, it is confirmed that miR24-2 is a microRNA with cancerous function, which is shown at least in hLCSCs. We have also demonstrated that miR24-2 can alter several complex signaling pathways and tumor-associated protein kinase functions in hLCSCs by affecting histone H3/4 epigenetic modification and cellular autophagy events.

RESULTS

miR24-2 Promotes the Growth of hLCSCs

To investigate the effects of miR24-2 on hLCSCs, hLCSCs were isolated from hLCSC line (Figures S2A–S2D; Supplemental Results). In the hLCSCs, the pCMV-miR and pCMV-miR24-2 were separately

Received 10 May 2019; accepted 18 October 2019;
https://doi.org/10.1016/j.ymthe.2019.10.015.

[3]These authors contributed equally to this work.

Correspondence: Dongdong Lu, Shanghai Putuo District People's Hospital, School of Life Science and Technology, Tongji University, Shanghai 200092, China.
E-mail: ludongdong@tongji.edu.cn

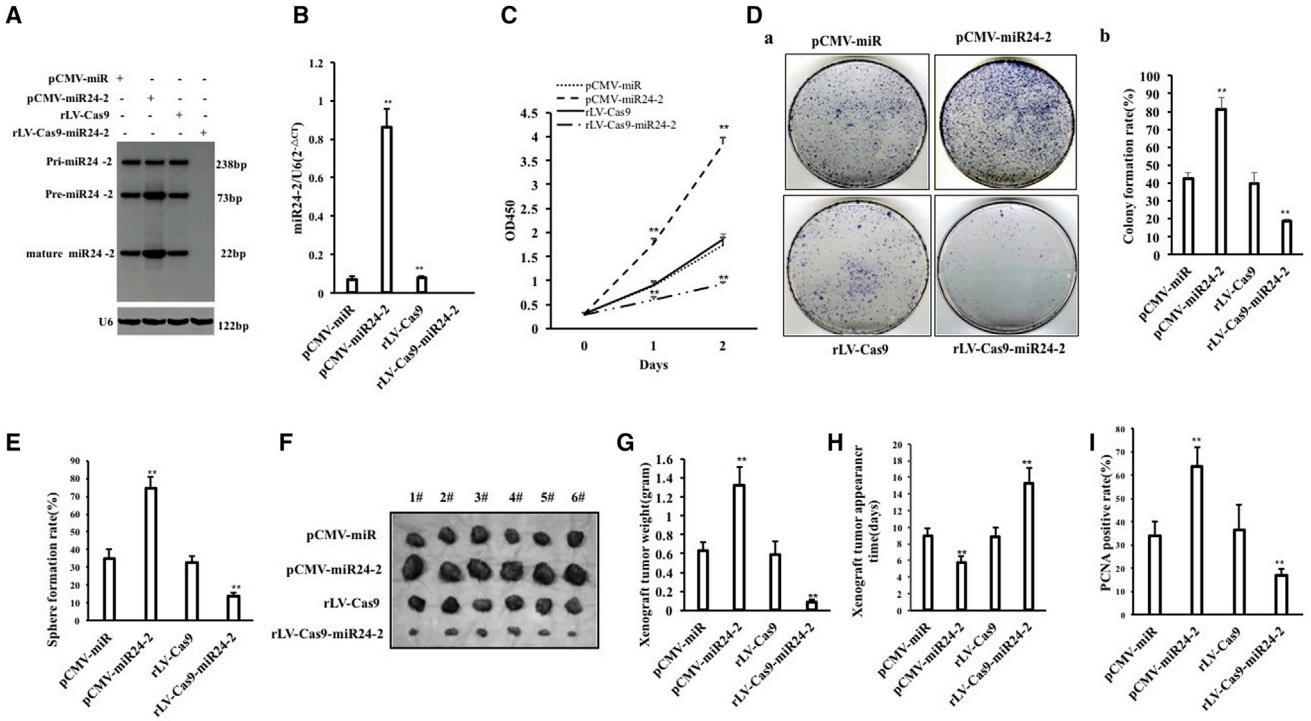

Figure 1. miR24-2 Promotes Growth of hLCSCs

(A) pCMV-miR or pCMV-miR24-2 were transfected into and the rLV-Cas9 or rLV-Cas9-miR24-2 were infected hLCSCs, respectively. Northern blotting was used to detect the miR24-2. U6 was used as an internal reference. (B) Quantitative RT-PCR was used to detect the miR24-2. U6 was used as an internal reference. (C) Cell proliferation ability was measured by the CCK8 method. $^{**}p < 0.01$, $^{*}p < 0.05$. (D) The plate colony formation ability of cells. (a) Photograph of plate colonies. (b) Determination of cell plate colony formation rate. $^{**}p < 0.01$, $^{*}p < 0.05$. (E) The sphere formation ability of cells. (F) hLCSCs cells were inoculated into BALB/c nude mice for 1 month. The photograph of the dissected xenograft is shown. (G) Comparison of the size (g) of transplanted tumors in nude mice (n = 6), $^{**}p < 0.01$, $^{*}p < 0.05$. (H) Comparison of time (days) of transplanted tumors in nude mice. (I) 4% formalin-fixed, paraffin-embedded nude mouse transplanted tumor tissue sections (4 μm) were subjected to the immunohistochemical staining of anti-PCNA. Comparison of PCNA-positive rates. $^{**}p < 0.01$, $^{*}p < 0.05$.

transfected and rLV-Cas9 and rLV-Cas9-miR24-2 were separately infected. The GFP or Green was expressed in four stable cell lines (pCMV-miR-hLCSCs, pCMV-miR24-2-hLCSCs, rLV-Cas9-hLCSCs, rLV-Cas9-miR24-2-hLCSCs), respectively (Figure S2A). In rLV-Cas9-miR24-2-hLCSCs, the 18 cases of hLCSCs stable cell lines were analyzed and showed that #2, #3, #6, #8, #11, #14, #15, and #16 were positive miR24-2 knockout cell lines (Figure S3). miR24-2 and cyclic miR24-2 were significantly increased in pCMV-miR24-2 group compared to the pCMV-miR group and reduced in rLV-Cas9-miR24-2 group compared to the rLV-Cas9 group (Figures 1A and 1B; Figures S2B and S2C). As shown in Figure 1A, the size of mature miR24-2 is 22 bp, the size of pre-miR24-2 is 73 bp, the size of pri-miR24-2 is 238 bp. Moreover, the knockout of miR-24-2 did not affect the expression of miR-23a and miR-27a in LCSCs (Figures S4A and S4B). Next, the cell proliferation index was significantly increased in pCMV-miR24-2 group compared with the pCMV-miR group (24 h, $p = 0.0056$; 48 h, $p = 0.0037$), and reduced in rLV-Cas9-miR24-2 group compared with the rLV-Cas9 group (24 h, $p = 0.0082$; 48, $p = 0.0051$) (Figure 1C). The colony formation rate was significantly increased in pCMV-miR24-2 compared with the pCMV-miR group (42.63% ± 3.03% versus 81.26% ± 6.61%, $p = 0.009978$) and reduced in the rLV-Cas9-miR24-2 group compared to the rLV-Cas9 group (39.82% ± 5.69% versus 18.41% ± 1.36%, $p = 0.00773$) (Figure 1D, a and b). The sphere formation rate was significantly increased in the pCMV-miR24-2 group compared with the pCMV-miR group (34.84% ± 5.23% versus 74.52% ± 6.51%, $p = 0.0082$) and reduced in the rLV-Cas9-miR24-2 group compared with the rLV-Cas9 group (32.56% ± 3.79% versus 13.78% ± 2.08%, $p = 0.0098$) (Figure 1E). Furthermore, miR24-2 increased the bromodeoxyuridine (BrdU)-positive rate (Figure S2D; Supplemental Results) and the average width ratio of scratches (Figure S2E; Supplemental Results). Moreover, the average weight of the transplanted tumors was significantly increased in the pCMV-miR24-2 group compared with the pCMV-miR group (0.63 ± 0.09 g versus 1.315 ± 0.194 g, $p = 0.0008042$) and decreased in the rLV-Cas9-miR24-2 group compared to the rLV-Cas9 group (0.598 ± 0.14 g versus 0.092 ± 0.0194 g, $p = 0.000202$) (Figures 1F and 1G). The average appearance time of transplanted tumors was significantly reduced in the pCMV-miR24-2 group compared with the pCMV-miR group (9.01 ± 0.89 days versus 5.83 ± 0.75 days, $p = 0.0000037$) and increased in the rLV-Cas9-miR24-2 group compared to rLV-Cas9

group (8.83 ± 1.17 days versus 15.33 ± 1.86 days, p = 0.00094) (Figure 1H). The poorly differentiated cancer cells were increased in the pCMV-miR24-2 group compared with the pCMV-miR group and decreased in the rLV-Cas9-miR24-2 group compared to the rLV-Cas9 group (Figure S2F). Furthermore, the proliferating cell nuclear antigen (PCNA)-positive rate was significantly increased in the pCMV-miR24-2 group compared with the pCMV-miR group (33.88% ± 6.31% versus 63.65% ± 8.46%, p = 0.00019) and reduced in the rLV-Cas9-miR24-2 group compared with the rLV-Cas9 group (36.56% ± 10.69% versus 76.82% ± 3.03%, p = 0.00343) (Figure 1I; Figure S2G). Moreover, the similar results were obtained in hLCSCs infected with rLV-tet on-miR24-2, including DOX (0 μg/mL) group, DOX (0.5 μg/mL) group, DOX (1 μg/mL) group, and DOX (2 μg/mL) group (Figures S2H–S2L; Supplemental Results). Collectively, these observations suggest that miR24-2 accelerates the growth of liver cancer stem cells *in vitro* and *in vivo*.

miR24-2 Targets PRMT7

To investigate whether miR24-2 targets PRMT7 in hLCSCs, we constructed four stable cell lines (pCMV-miR-hLCSCs, pCMV-miR24-2-hLCSCs, rLV-Cas9-hLCSCs, rLV-Cas9-miR24-2-hLCSCs) (Figure S5A, a and b). Bioinformatics analysis revealed that the mature sequence of miR24-2 binds to the 3′ UTR of PRMT7 mRNA (2627-2648) via a 12-base complementary seed sequence (Figure 2A). Compared with the pCMV-miR group, the pEZX-MT-PRMT7 3′ UTR-Luc luciferase reporter gene activity was significantly reduced in the pCMV-miR24-2 group (p = 0.00126) and increased in the rLV-Cas9-miR24-2 group compared with the rLV-Cas9 group (p = 0.00581) (Figure 2B). However, there was no significant change of the pEZX-MT-PRMT7 3′ UTR(mutante)-Luc reporter gene activity among the four groups (p > 0.05) (Figure S5B). Although there was no significant change in the transcription level of PRMT7, the translational level of PRMT7 was significantly reduced in the pCMV-miR24-2 group compared to the pCMV-miR group and increased in the rLV-Cas9-miR24-2 group compared to the rLV-Cas9 group (Figure 2C). Furthermore, the similar results were obtained in hLCSCs infected with rLV-tet on-miR24-2, including DOX (0 μg/mL) group, DOX (0.5 μg/mL) group, DOX (1 μg/mL) group, and DOX (2 μg/mL) group (Figures S5C–S5G; Supplemental Results). Taken together, these results suggest that miR24-2 targets PRMT7 3′ UTR and inhibits the expression of the PRMT7 in hLCSCs.

miR24-2 Enhances the Expression of Nanog

Given that miR24-2 inhibits the expression of PRMT7, we consider whether miR24-2 reduces H4R3 methylation modification in hLCSCs. The interaction between histone H4 and PRMT7 was attenuated in the pCMV-miR24-2 group compared with the pCMV-miR group and enhanced in the rLV-Cas9-miR24-2 group compared with the rLV-Cas9 group (Figure 2D). The modification of H4R3me2 or H4R3me3 was significantly reduced in the pCMV-miR24-2 group compared with the pCMV-miR group and increased the rLV-Cas9-miR24-2 group compared with the rLV-Cas9 group. However, the modification of H4R3me was not significantly changed in these groups (Figure 2E). Moreover, the modification of H4R3me2 or H4R3me3 was significantly not altered in the pCMV-miR24-2-+pcDNA3-PRMT7 group compared to pCMV-miR group (Figure 2F). Furthermore, the modification of dimethylation and trimethylation of arginine-3 of histone H4 on the long noncoding RNA HULC promoter region was significantly reduced in the pCMV-miR24-2 group compared with the pCMV-miR group and increased in the rLV-Cas9-miR24-2 group compared with the rLV-Cas9 group (Figure 2G). Notably, miR24-2 affects the modification of trimethylation of arginine-3 of histone H4 on the HULC promoter region specifically (Figure S6; Supplemental Results). Furthermore, the pGL4-HULC-Luc luciferase reporter activity was significantly increased in the pCMV-miR24-2 group compared with the pCMV-miR group (p = 0.00183) and reduced in the rLV-Cas9-miR24-2 group compared to the rLV-Cas9 group (p = 0.00447) (Figure 2H). Therefore, the HULC was significantly increased in the pCMV-miR24-2 group compared to the pCMV-miR group and reduced in the rLV-Cas9-miR24-2 group compared to the rLV-Cas9 group (Figure 2I). However, the HULC was significantly not altered in the pCMV-miR24-2+pcDNA3-PRMT7 group compared to pCMV-miR group (Figure 2J). In particular, the binding ability of KLF4, C-myc, and Epcam to HULC was significantly enhanced in the pCMV-miR24-2 group compared with the pCMV-miR group and weakened in the rLV-Cas9-miR24-2 group compared with the rLV-Cas9 group (Figure 3A). Moreover, the binding ability of Ecamp to C-myc, C-myc to Epcam, and KLF4 to C-myc was significantly enhanced in the pCMV-miR24-2 group compared with the pCMV-miR group and weakened in the rLV-Cas9-miR24-2 group compared with the rLV-Cas9 group, respectively (Figure 3B). However, the binding ability of Ecamp to C-myc, C-myc to Epcam, and KLF4 to C-myc was significantly not altered in the pCMV-miR24-2+pGFP-V-RS-HULC group compared with the pCMV-miR group (Figure 3C). Thereby, the binding ability of C-myc, Epcam, and KLF4 to the Nanog promoter was significantly enhanced in the pCMV-miR24-2 group compared with the pCMV-miR group and weakened the rLV-Cas9-miR24-2 group compared with the rLV-Cas9 (Figure 3D). However, there was no significant change in the binding ability of C-myc, Epcam, and KLF4 to the Nanog promoter in the pCMV-miR24-2+pGFP-V-RS-HULC group compared to the pCMV-miR group, respectively (Figure 3E). Furthermore, the pEZX-MT-Nanog-Luc luciferase reporter gene activity was significantly enhanced in the pCMV-miR24-2 group compared to the pCMV-miR group (p < 0.01) and reduced in the rLV-Cas9-miR24-2 group compared to the rLV-Cas9 group (p < 0.01) (Figure 3F). However, there was no significant difference between the pCMV-miR24-2+pGFP-V-RS-HULC group and the pCMV-miR group (8,938.45 ± 1,261.59 versus 8,444.96 ± 1,055.63, p > 0.05) (Figure 3G). Ultimately, the expression of Nanog was significantly increased in the pCMV-miR24-2 group compared to the pCMV-miR group and reduced in the rLV-Cas9-miR24-2 group compared to the rLV-Cas9 group (Figure 3H). However, there was no significant difference between the pCMV-miR24-2+pGFP-V-RS-HULC group and the pCMV-miR group (Figure 3I). Collectively, these results suggest that miR24-2 enhances the expression of Nanog in hLCSCs.

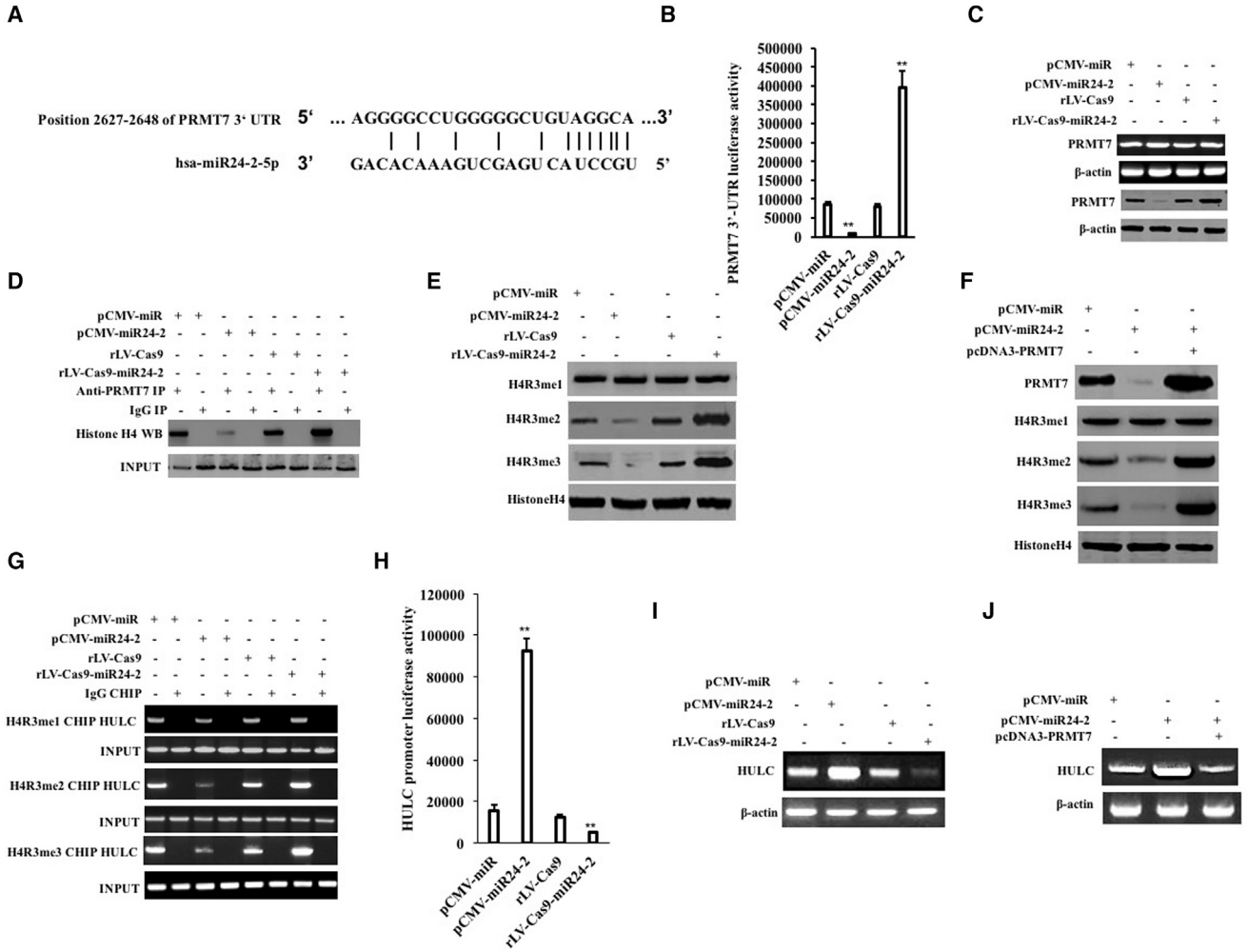

Figure 2. miR24-2 Targets PRMT7 and Inhibits HULC in hLCSCs

(A) Bioinformatics method to analyze binding seed sequences of mature miR24-2 to PRMT7 mRNA 3′ UTR. (B) The cells were tested for pEZX-MT-PRMT7 3′ UTR-Luc dual luciferase reporter gene activity. $^{**}p < 0.01$, $^{*}p < 0.05$. (C) The PRMT7 was detected by RT-PCR and western blotting. β-actin was used as an internal reference gene. (D) CoIP with anti-PRMT7 was performed and the precipitate was analyzed by western blotting with anti-histone H4. Immunoglobulin G (IgG) coIP was used as a negative control and western blotting anti-PRMT7 was subjected to as INPUT. (E) Western blotting using anti-H4R3me, anti-H4R3me2, and anti-H4R3me3 was performed, and β-actin was used as an internal reference gene. (F) Western blotting using anti-H4R3me, anti-H4R3me2, and anti-H4R3me3 was performed, and β-actin was used as an internal reference gene. (G) ChIP using anti-H4R3me, anti-H4R3me2, and anti-H4R3me3. PCR amplification was carried out using primers designed according to the HULC promoter. IgG ChIP was used as a negative control and the product amplified by the primer designed by the HULC promoter was used as an internal reference (INPUT). (H) The pGL4-HULC-Luc luciferase reporter gene activity was measured. $^{**}p < 0.01$, $^{*}p < 0.05$. (I) HULC was analyzed by RT-PCR. (J) HULC was analyzed by RT-PCR. β-actin was used as an internal reference gene.

miR24-2 Promotes the Expression and Maturation of miR675 via Nanog

To analyze whether miR24-2 affects the binding ability of Nanog to the miR675 precursor promoter, we first analyzed this binding ability of Nanog to the miR675 promoter *cis* element using a super-gel migration assay. The binding ability of Nanog to the pri-miR675 promoter cis-element probe was significantly enhanced in the pCMV-miR24-2 group compared with the pCMV-miR group and reduced the rLV-Cas9-miR24-2 group compared with the rLV-Cas9 group (Figure 4A, a and b). Moreover, the binding ability of Nanog to pri-miR675 promoter was significantly enhanced in the pCMV-miR24-2 group compared with the pCMV-miR group and attenuated in rLV-Cas9-miR24-2 group compared with the rLV-Cas9 group (Figure 4B). However, there was no significant change between the pCMV-miR24-2+pGFP-V-RS-HULC group and the pCMV-miR group (Figure 4C). Furthermore, the pri-miR675 promoter luciferase reporter gene activity was significantly increased in the pCMV-miR24-2 group compared with the pCMV-miR group

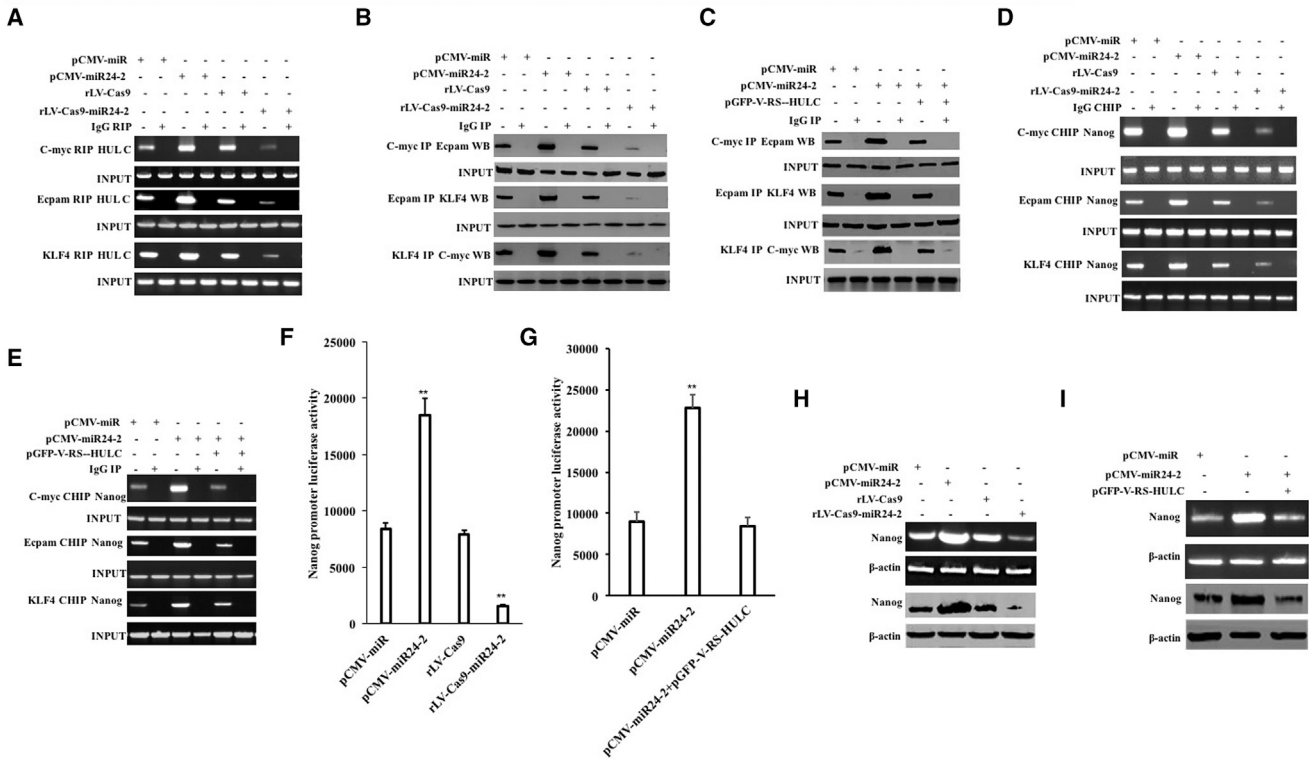

Figure 3. miR24-2 Promotes the Expression of Nanog in Human Liver Stem Cells

(A) The RIP using anti-KLF7, anti-C-myc, anti-Epcam. The HULC sequence was designed to amplify the HULC by RT-PCR. IgG RNA immunoprecipitation (RIP) was used as a negative control. (B) Immunoprecipitation using anti-C-myc, anti-Epcam, and anti-KLF4, respectively. (C) The coIP with anti-C-myc, anti-Epcam, and anti-KLF4, respectively. (D) ChIP using anti-C-myc, anti-Epcam, and anti-KLF4. IgG ChIP was used as a negative control. (E) The ChIP using anti-C-myc, anti-Epcam, and anti-KLF4. (F) The pEZX-MT-Nanog-Luc luciferase reporter gene activity was assayed. (G) The pEZX-MT-Nanog-Luc luciferase reporter gene activity was detected. $^{**}p < 0.01$, $^{*}p < 0.05$. (H) The Nanog was analyzed by RT-PCR and western blot. β-actin was used as an internal reference gene. (I) The Nanog was analyzed by RT-PCR and western blotting. β-actin was used as an internal reference gene.

($p = 0.0009519$) and reduced in the rLV-Cas9-miR24-2 group compared to the rLV-Cas9 group ($p = 0.007702$) (Figure 4D). However, there was no significant change between the pCMV-miR24-2+pGFP-V-RS-HULC group compared to the pCMV-miR group ($p = 0.400512 > 0.05$) (Figure 4E). Therefore, the pri-miR675, pre-miR675, and mature miR675 were significantly increased in the pCMV6-miR24-2 group compared with the pCMV-miR group and reduced in the rLV-Cas9-miR24-2 group compared to the rLV-Cas9 group (Figure 4F, a and b). However, there was no significant change between pCMV-miR24-2+pGFP-V-RS-HULC group and the pCMV-miR group (Figure 4G, a and b). Moreover, in hLCSCs infected with rLV-tet on-miR24-2, the transcriptional activity of pri-miR675 was significantly increased with increasing DOX concentration (Figures 4H and 4I; Figures S7A–S7G; Supplemental Results). Furthermore, the binding ability of Drosha pol III, DGCR8, and Exportin5 to pri-miR675 was significantly increased (Figures 4J and 4K) and pri-miR675, pre-miR675, and mature miR675 were significantly increased with increasing DOX concentration (Figure 4L, a and b). Collectively, these results suggest that miR24-2 increases miR675 through Nanog hLCSCs.

miR24-2 Enhances Acetylation on H4K16 and Inhibits Methylation on H4K20

Given that miR675 targets HDAC3 3′ UTR and and inhibits expression of the *HDAC3* gene in hLCSCs (Figures S8A–S8F; Supplemental Results), we consider whether miR24-2 promotes acetylation of the 16th lysine of histone H4 and inhibits methylation of the 20th lysine of histone H4 via miR675. The expression of HDAC3 was significantly reduced in the pCMV6-miR24-2 group compared to the pCMV-miR group and increased in the rLV-Cas9-miR24-2 group compared to the rLV-Cas9 group (Figure 5A). However, there was no significant change between the pCMV-miR24-2+miR675 inhibitor group compared to the pCMV-miR group (Figure 5B). The expression of HDAC3 was significantly reduced as the concentration of increased DOX in the DOX (0 μg/mL) group, DOX (0.5 μg/mL) group, DOX (1 μg/mL) group, DOX (1.5 μg/mL) group, and DOX (2 μg/mL) group (Figure 5C). However, there was no significant change as the increasing DOX concentration among the hLCSCs of DOX (0 μg/mL)/miR675 inhibitor group, DOX (1 μg/mL)/miR675 inhibitor group, and DOX (2 μg/mL)/miR675 inhibitor group (Figure 5D). Furthermore, the interaction of histone H4 with HDAC3

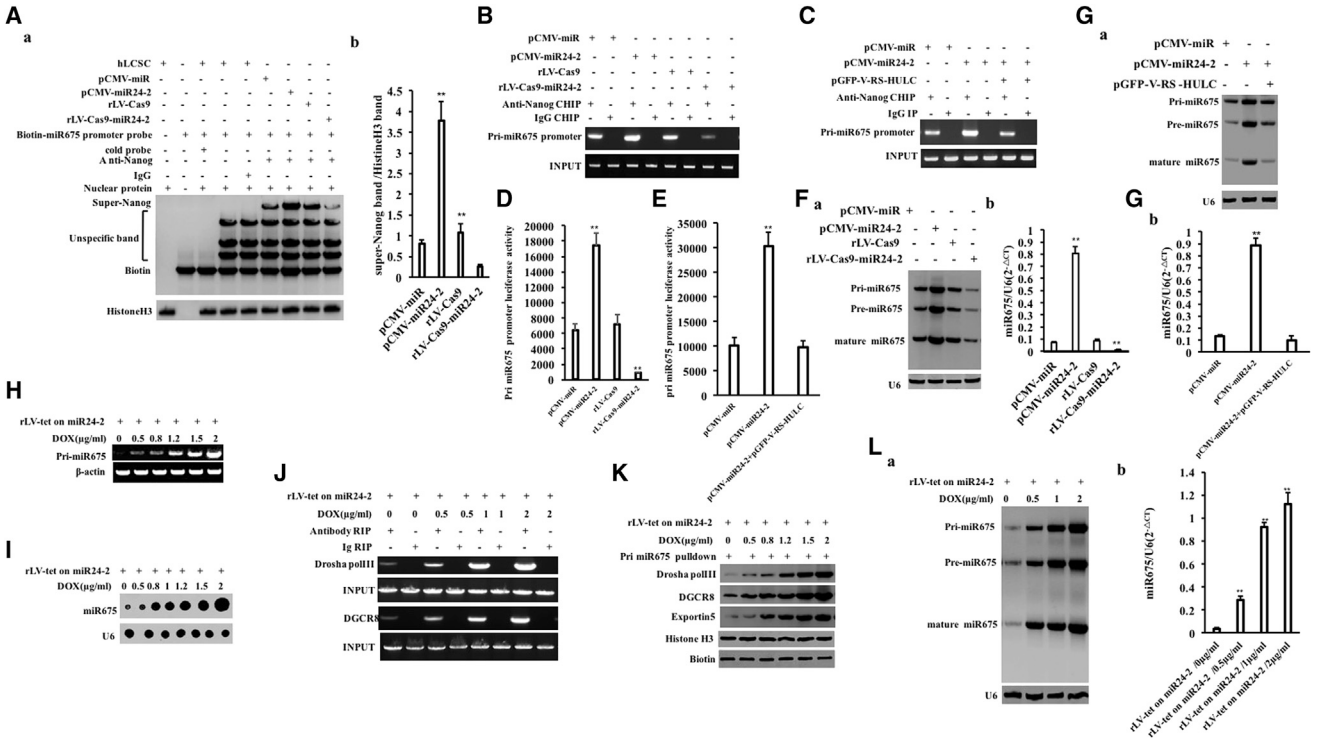

Figure 4. miR24-2 Promotes Expression and Maturation of miR675

(A) (a) Super-DNA-protein complex gel migration assay using biotin-labeled pri-miR675 promoter *cis*-element probe and anti-Nanog, anti-Biotin. IgG super-EMSA was used as a negative control. (b) Grayscale scan analysis of positive bands. (B) The ChIP using anti-Nanog. The PCR amplification was carried out using a primer designed according to the pri-miR675 promoter. (C) The ChIP using anti-Nanog. (D) The pEZX-MT-pri-miR675-Luc luciferase reporter activity was assayed. $^{**}p < 0.01$, $^{*}p < 0.05$. (E) The pEZX-MT-pri-miR675-Luc luciferase reporter gene activity was detected. (F) (a) Northern blotting was used to detect the miR675. U6 was used as an internal reference gene. (b) Quantitative RT-PCR analysis. (G) (a) Northern blotting was used to detect the miR675. U6 was used as an internal reference gene. (b) Quantitative RT-PCR. (H) The pri-miR675 was analyzed by RT-PCR. β-actin is used as an internal reference. (I) The miR675 was analyzed by dot blotting. U6 is used as an internal reference. (J) RIP with anti-Drosha pol III and anti-DGCR8 was performed. IgG RNA immunoprecipitation was used as a negative control. (K) RNA pulldown was performed. Biotin was used as INPUT and histone H3 was as an internal reference. (L) (a) miR675 was detected by Northern blotting. U6 serves as an internal reference gene. (b) Detection of miR675 by quantitative RT-PCR. U6 was used as an internal reference gene. $^{**}p < 0.01$, $^{*}p < 0.05$.

was significantly attenuated in the pCMV-miR24-2 group compared to the pCMV-miR group and enhanced in the rLV-Cas9-miR24-2 group compared to the rLV-Cas9 group (Figure 5E). In stable hLCSCs infected with rLV-tet on-miR24-2, the interaction between histone H4 and HDAC3 was significantly reduced with increasing DOX concentration (Figure 5F). The level of H4K16Ac was significantly increased in the pCMV6-miR24-2 group compared to the pCMV-miR group and reduced in the rLV-Cas9-miR24-2 group compared to the rLV-Cas9 group (Figure 5G). However, there was no significant change of H4K16Ac between the pCMV6-miR24-2+miR675 inhibitor group and pCMV-miR group (Figure 5H). The H4K16Ac was significantly increased with increasing DOX concentration in DOX (0 μg/mL) group, DOX (0.5 μg/mL) group, DOX (0.8 μg/mL) group, DOX (1.2 μg/mL) group, DOX (1.5 μg/mL) group, and DOX (2 μg/mL) group (Figure 5I). However, H4K16Ac did not change significantly with increasing DOX concentration among DOX (0 μg/mL)/miR675 inhibitor group, DOX (1 μg/mL)/miR675 inhibitor group, and DOX (2 μg/mL)/miR675 inhibitor group (Figure 5J). Furthermore, the level of H4K16Ac was significantly increased and the levels of HDAC3, H4K20me1/2/3, and H3K79me3 H3K79me3 were significantly decreased in the pCMV-miR24-2 group compared with the pCMV-miR group. However, there was no significant change between pCMV-miR24-2+pcDNA3-HDAC3 group and the pCMV-miR group (Figure 5K). However, HDAC3, H4K16Ac, H4K20me1/2/3, and H3K79me3 H3K79me3 did not significantly change with increasing DOX concentration in the DOX (0 μg/mL)/pcDNA3-HDAC3 group, the DOX (1 μg/mL)/pcDNA3-HDAC3 group, and the DOX (2 μg/mL)/pcDNA3-HDAC3 group (Figure 5L). Collectively, these results suggest that miR24-2 promotes acetylation on the 16th lysine of histone H4 and inhibits methylation on the 20th lysine of histone H4 by miR675-HDAC3.

miR24-2 Enhances the Expression of Phosphatidylinositol 3-Kinase

To analyze whether miR24-2 affects the modification of histone H4K16Ac and H4K20me2 on the phosphatidylinositol 3-kinase (PI3K) promoter region, we first performed chromatin immunoprecipitation (ChIP) analysis in hLCSCs. The modification of H4K16Ac

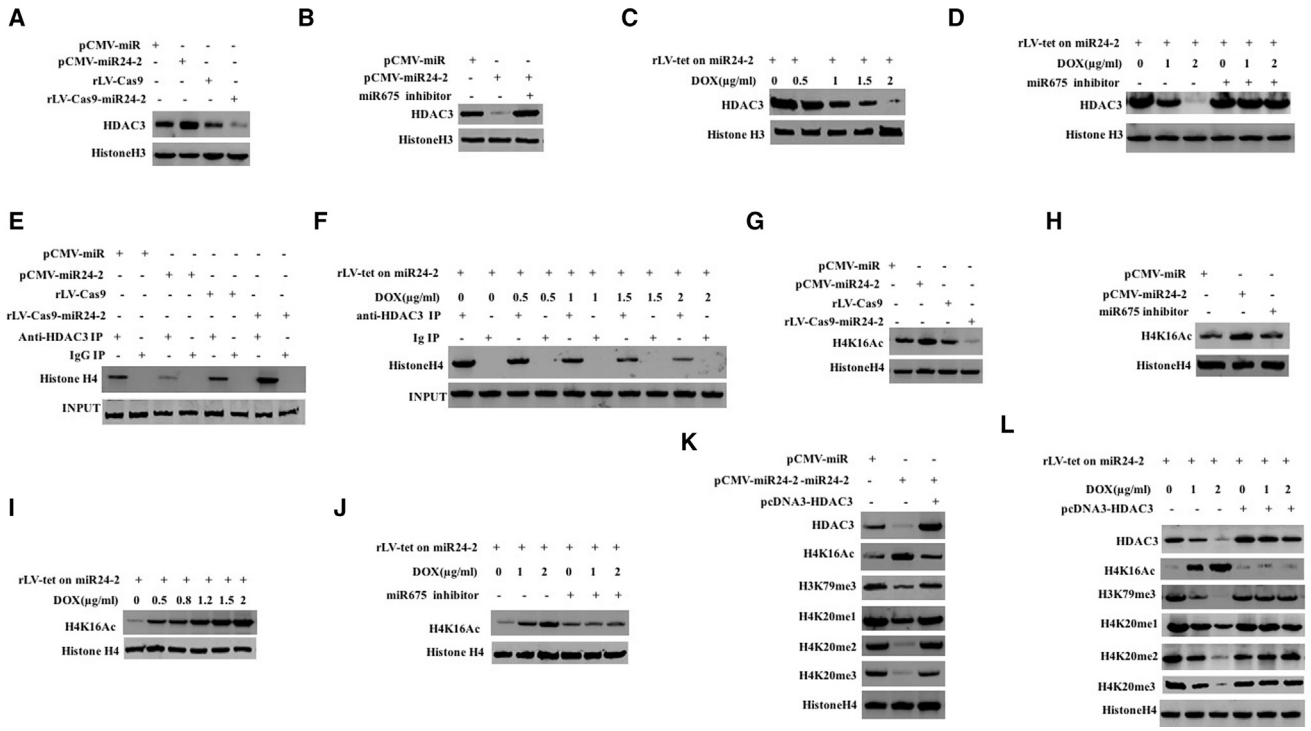

Figure 5. miR24-2 Promotes Acetylation of the 16th Lysine of Histone H4 and Inhibits Methylation of the 20th Lysine of Histone H4 in hLCSCs

(A) HDAC3 was detected by western blotting. β-actin was used as an internal reference gene. (B) HDAC3 was detected by western blotting. (C) HDAC3 was detected by western blotting. β-actin was used as an internal reference gene. (D) The HDAC3 was detected by western blotting. β-actin is used as an internal reference gene. (E) CoIP was performed using anti-HDAC3. IgG coIP was used as a negative control. (F) CoIP was performed using anti-HDAC3. (G) Western blotting was used to detect the H4K16Ac. (H) The H4K16Ac was detected by western blotting. (I) The H4K16Ac was detected by western blotting. Histone H4 serves as an internal reference gene. (J) The H4K16Ac was detected by western blotting. (K) Western blotting was used to detect HDAC3, H4K16Ac, H4K20me1/2/3, and H3K79me3 H3K79me3. (L) Western blotting was used to detect HDAC3, H4K16Ac, H4K20me1/2/3, and H3K79me3 H3K79me3. Histone H4 was used as an internal reference gene.

in the PI3K promoter region was significantly increased in the pCMV-miR24-2 group compared with the pCMV-miR group and reduced in the rLV-Cas9-miR24-2 group compared with the rLV-Cas9 group, and the modification of H4K20me2 in the PI3K promoter region was significantly decreased in the pCMV-miR24-2 group compared with the pCMV-miR group and increased in the rLV-Cas9-miR24-2 group compared with the rLV-Cas9 group (Figure 6A). In hLCSCs infected with rLV-tet on-miR24-2, the modification of H4K16Ac in the PI3K promoter region was significantly increased and the modification of H4K20me2 in the PI3K promoter region was significantly decreased with increasing DOX concentration (Figure S9A). The pGL4-PI3K-Luc luciferase reporter gene activity was significantly increased in the pCMV-miR24-2 group compared with the pCMV-miR group ($p = 0.00195$) and reduced in the rLV-Cas9-miR24-2 group compared to the rLV-Cas9 group ($p = 0.0052453$) (Figure 6B). The PI3K luciferase reporter gene activity was increased with increasing DOX concentration in the DOX (0 μg/mL) group, the DOX (0.5 μg/mL) group, DOX (1.0 μg/mL) group, DOX (1.5 μg/mL) group, and DOX (2 μg/mL) group ($p < 0.01$) (Figure S9B). The PI3K expression was significantly increased in the pCMV-miR24-2 group compared to the pCMV-miR group and reduced in the rLV-Cas9-miR24-2 group compared to the rLV-Cas9 group (Figures 6C and 6D). And the expression of PI3K was significantly increased as the increasing DOX concentration In DOX (0 μg/mL) group, DOX (0.5 μg/mL) group, DOX (0.8 μg/mL) group, DOX (1.2 μg/mL) group, DOX (1.5 μg/mL) group, and DOX (2 μg/mL) group (Figures S9C and S9D). Furthermore, the binding ability of H3K20me2 to the PI3K promoter *cis*-element probe was significantly reduced with increasing DOX concentration in hLCSCs infected with rLV-tet on-miR24-2. However, the binding ability of H3K20me2 to the PI3K promoter *cis*-element probe did not significantly change with increasing DOX concentration among rLV-tet on-miR24-2/DOX (0 μg/mL) +pcDNA3-HDAC3 group, rLV-tet on-miR24-2/DOX (1 μg/mL) +pcDNA3-HDAC3 group, and rLV-tet on-miR24-2+pcDNA3-HDAC3/DOX (2 μg/mL) group (Figure S10A, a and b). Moreover, the binding capacity of RNA polII to PI3K promoter *cis*-element probes was significantly increased with increasing DOX concentration. However, the binding ability of RNA polII to the PI3K promoter *cis*-element probe did not significantly change with increasing DOX concentration in rLV-tet on-miR24-2/DOX (0 μg/mL) +pcDNA3-HDAC3 group, rLV-tet on-miR24-2/DOX (1 μg/mL) +pcDNA3-HDAC3 group, and rLV-tet

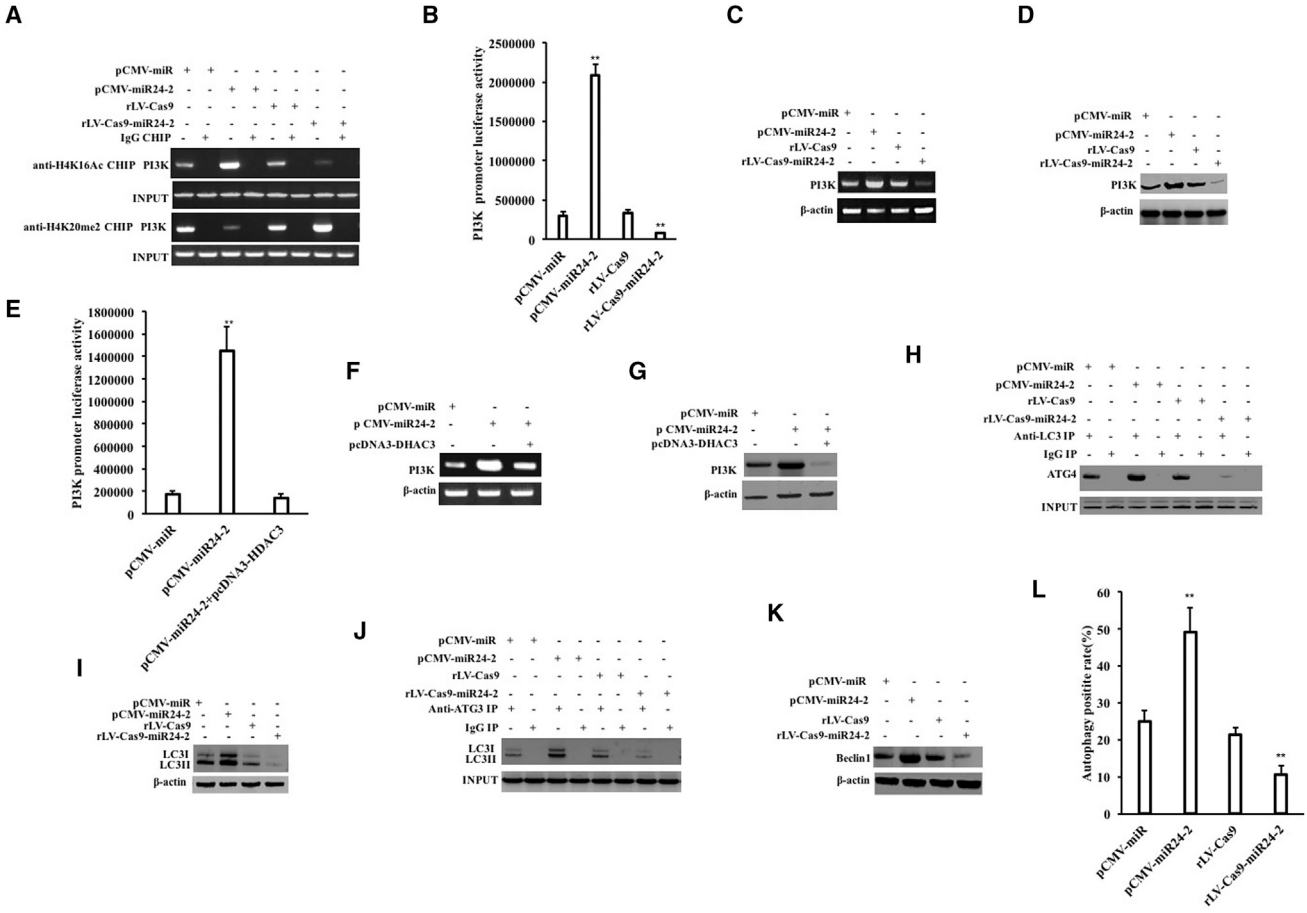

Figure 6. miR24-2 Enhances PI3K and Affects Autophagy in hLCSCs

(A) The ChIP using anti-H4K6Ac and anti-H4K20me2. IgG ChIP was used as a negative control. (B) The pGL4-PI3K-Luc luciferase reporter gene activity was tested. (C) RT-PCR was performed using PI3K primers. (D) Western blotting using anti-PI3K. β-actin was used as an internal reference gene. (E) The pGL4-PI3K-Luc luciferase reporter gene activity was detected. $^{**}p < 0.01$, $^{*}p < 0.05$. (F) The RT-PCR was performed. (G) The total protein was subjected to western blotting using anti-PI3K. β-actin was used as an internal reference gene. (H) The coIP with anti-LC3. IgG coIP was used as a negative control. (I) Western blotting using anti-LC3. β-actin as an internal reference gene. (J) The coIP with anti-ATG3. (K) Western blotting using anti-Beclin1. β-actin as an internal reference gene. (L) The infection of adenovirus rAd-Cherry-GFP-LC3 can monitor the autophagy through fluorescence microscopy directly. The occurrence of autophagy was observed (red marker Cherry-LC3). Comparison of the incidence of autophagy. $^{**}p < 0.01$, $^{*}p < 0.05$.

on-miR24-2/DOX (2 μg/mL)+pcDNA3-HDAC3 group (Figure S10B, a and b). The pGL4-PI3K-Luc luciferase reporter gene activity was significantly increased in the pCMV-miR24-2 group compared with the pCMV-miR group ($p = 0.004232$). However, there was no significant difference between the pCMV-miR24-2+pcDNA3-HDAC3 group ($p = 0.223619$) (Figure 6E). The PI3K promoter luciferase reporter gene activity was significantly increased with increasing DOX concentration among rLV-tet on-miR24-2/DOX (0 μg/mL) group, rLV-tet on-miR24-2/DOX (1 μg/mL) group, and rLV-tet on-miR24-2/DOX (2 μg/mL) group ($p < 0.01$). However, the PI3K promoter luciferase reporter gene activity did not change significantly with increasing DOX concentration in rLV-tet on-miR24-2/DOX (0 μg/mL) +pcDNA3-HDAC3 group, rLV-tet on-miR24-2/DOX (1 μg/mL) +pcDNA3-HDAC3 group, rLV-tet on-miR24-2/DOX (2 μg/mL) +pcDNA3-HDAC3 group ($p > 0.05$) (Figure S10C). Moreover, the expression of PI3K transcriptional capacity was significantly increased in the pCMV6-miR24-2 group compared to the pCMV-miR group. However, there was no significant change between the pCMV-miR24-2+pcDNA3-HDAC3 group and the pCMV-miR group (Figures 6F and 6G). The expression of PI3K was significantly increased in the DOX (2 μg/mL) group compared to the DOX (0 μg/mL) group. However, there was no significant change between the rLV-tet on-miR24-2/DOX (2 μg/mL) +pcDNA3-HDAC3 group and the rLV-tet on-miR24-2/DOX (0 μg/mL) (Figures S9E and S9F). The expression of PI3K/H4K16Ac was significantly increased and H3K20me2/KAT8 was significantly decreased, and SET8 did not significantly change in the pCMV-miR24-2 group compared with the pCMV-miR group. However, there was no significant change between the pCMV-miR24-2+pGFP-V-RS-KAT8 group or the pCMV-miR24-2-+pcDNA3-SET8 group compared with the pCMV-miR group (Figures S10D and S10F). The expression of PI3K/H4K16Ac was

significantly increased and H3K20me2/KAT8 was significantly decreased and SET8 did not change in the DOX (2 μg/mL) group compared with the DOX (0 μg/mL) group. However, there was no significant change in rLV-tet on-miR24-2/DOX (2 μg/mL) +pGFP-V-RS-KAT8 or rLV-tet on-miR24-2/DOX (2 μg/mL) +pcDNA3-SET8 group compared with the rLV-tet on-miR24-2/DOX (0 μg/mL) group (Figures S10E and S10G). Collectively, these results suggest that miR24-2 promotes expression of PI3K via HDAC3-H4K16Ac -H4K20me2 in hLCSCs.

miR24-2 Promotes Cellular Autophagy Dependent on PI3K

Given that miR24-2 promotes the expression of PI3K and that PI3K can cause cellular autophagy in several cells, we consider whether miR24-2 promotes autophagy of hLCSCs. First, the interaction between the autophagy structural protein LC3 and the LC3 cleavage protein ATG4 was enhanced in the pCMV-miR24-2 group compared to the pCMV-miR group and weakened in rLV-Cas9-miR24-2 group compared to the rLV-Cas9 group (Figure 6H). In the hLCSCs infected with rLV-tet on-miR24-2, the interaction of LC3 with ATG4 was significantly increased as the increasing concentration of DOX (Figure S9G). The expression of LC3I and LC3II was significantly increased in the pCMV-miR24-2 group compared to the pCMV-miR group and reduced in the rLV-Cas9-miR24-2 group to the rLV-Cas9 group (Figure 6I). Moreover, the expression of LC3I and LC3II increased significantly as the DOX concentration increased in DOX (0 μg/mL) group, DOX (0.5 μg/mL) group, DOX (0.8 μg/mL) group, DOX (1.2 μg/mL) group, DOX (1.5 μg/mL) group, and DOX (2 μg/mL) group (Figure S9H). And the interaction between the LC3 and ATG3 was enhanced in the pCMV-miR24-2 group compared to the pCMV-miR group and significantly attenuated in the rLV-Cas9-miR24-2 group compared to the rLV-Cas9 group (Figure 6J). Moreover, the interaction of LC3 with ATG3 was significantly increased with the increasing concentration of DOX in DOX (0 μg/mL) group, DOX (0.5 μg/mL) group, and DOX (1 μg/mL) group, DOX (2 μg/mL) group (Figure S9I). The expression of the autophagy marker protein Beclin1 was significantly increased in the pCMV-miR24-2 group compared to the pCMV-miR group and significantly reduced in the rLV-Cas9-miR24-2 group compared to the rLV-Cas9 group (Figure 6K). The expression of Beclin1 was significantly increased with increasing DOX concentration significantly (Figure S9J). The incidence of autophagy was significantly increased in the pCMV-miR24-2 group compared with the pCMV-miR group (24.85% ± 3.01% versus 49.04% ± 6.59%, $p = 0.00762688$) and reduced in the rLV-Cas9-miR24-2 group compared with the rLV-Cas9 group (21.3% ± 2.06% versus 10.47% ± 2.46%, $p = 0.0223$) (Figure 6L; Figure S9K, b). Furthermore, the incidence rate of autophagy was significantly increased with increasing DOX concentration in the DOX (0 μg/mL) group, DOX (0.5 μg/mL) group, DOX (1.5 μg/mL) group, and DOX (2 μg/mL) ($p < 0.01$ or $p < 0.05$) (Figure S9L, a and b). Moreover, PI3K knockdown abrogates these actions of miR24-2 for autophagy (Figures S11A–S11I; Supplemental Results). Collectively, these results suggest that miR24-2 promotes autophagy dependent on PI3K in hLCSCs.

miR24-2 Promotes the Expression of PKM1 Dependent on Cellular Autophagy

In order to investigate the role of miR24-2-dependent autophagy in affecting the expression of PKM1, we first explored whether miR24-2 can enhance the interaction between PKM1 and autophagosome functional proteins in LCSCs. The interaction of PKM1 with the LC3I/II or the autophagy functional protein P62 was enhanced in the pCMV-miR24-2 group compared with the pCMV-miR group and attenuated in the rLV-Cas9-miR24-2 group compared to the rLV-Cas9 group (Figure 7A). The interaction between PKM1 and LC3I/II, and PKM1 and protein P62 were significantly enhanced with increasing DOX concentration in DOX (0 μg/mL) group, DOX (0.5 μg/mL) group, DOX (1 μg/mL) group, DOX (1.5 μg/mL) group, and DOX (2 μg/mL) group (Figure 7B). The expression of PKM1 was significantly increased in the pCMV-miR24-2 group compared to the pCMV-miR group and reduced in the rLV-Cas9-miR24-2 group compared to the rLV-Cas9 group (Figure 7C). Moreover, the expression of PKM1 was significantly increased as the DOX concentration increased in the DOX (0 μg/mL) group, DOX (0.5 μg/mL) group, DOX (0.8 μg/mL) group, DOX (1.2 μg/mL) group, DOX (1.5 μg/mL) group, and DOX (2 μg/mL) group (Figure 7D). The expression of PKM1 was significantly increased in the pCMV-miR24-2 group compared to the pCMV-miR group. However, there was no significant change between the pCMV-miR24-2+3-MA group and the pCMV-miR group (Figure 7E). The expression of PKM1 was significantly increased in the DOX (2 μg/mL) treated group compared to the DOX (0 μg/mL) group. However, there was no significant change between the rLV-tet on-miR24-2/DOX (2 μg/mL) +3-MA group and the DOX (0 μg/mL) group (Figure 7F). Collectively, these results suggest that miR24-2 enhances the expression of PKM1 dependent on autophagy in hLCSCs.

miR24-2 Enhances the Expression of Tyrosine Protein Kinase Sarcoma Gene *Src* by Enhancing PKM1

To analyze whether miR24-2 affects the expression of the tyrosine protein kinase sarcoma gene *Src* through PKM1, we performed a series of assays in LCSCs. The binding ability of PKM1 to *Src* promoter was significantly increased in the pCMV-miR24-2 group compared with the pCMV-miR group and reduced in the rLV-Cas9-miR24-2 group compared with the rLV-Cas9 group (Figure 7G). The binding ability of PKM1 and RNA polII to the Src promoter-enhancer loop were significantly increased in the pCMV-miR24-2 group compared with the pCMV-miR group and reduced in the rLV-Cas9-miR24-2 group compared with the rLV-Cas9 group (Figure 7H). Furthermore, the binding ability of PKM1 to *Src* promoter was significantly increased with the increasing DOX concentration (Figure 7I). The binding ability of PKM1, RNApolII, and *Src* promoter-enhancer loop was significantly increased with increasing DOX concentration in the DOX (0 μg/mL) group, the DOX (1 μg/mL) group, and the DOX (2 μg/mL) group (Figure 7J). The pGL4-Src-Luc luciferase reporter gene activity was significantly increased in the pCMV-miR24-2 group compared with the pCMV-miR group ($p = 0.004693$) and reduced in the rLV-Cas9-miR24-2 group compared to the rLV-Cas9 group ($p = 0.0061157$) (Figure 7K). The *Src* promoter luciferase reporter gene activity was increased with increasing DOX concentration ($p < 0.01$) (Figure 7L).

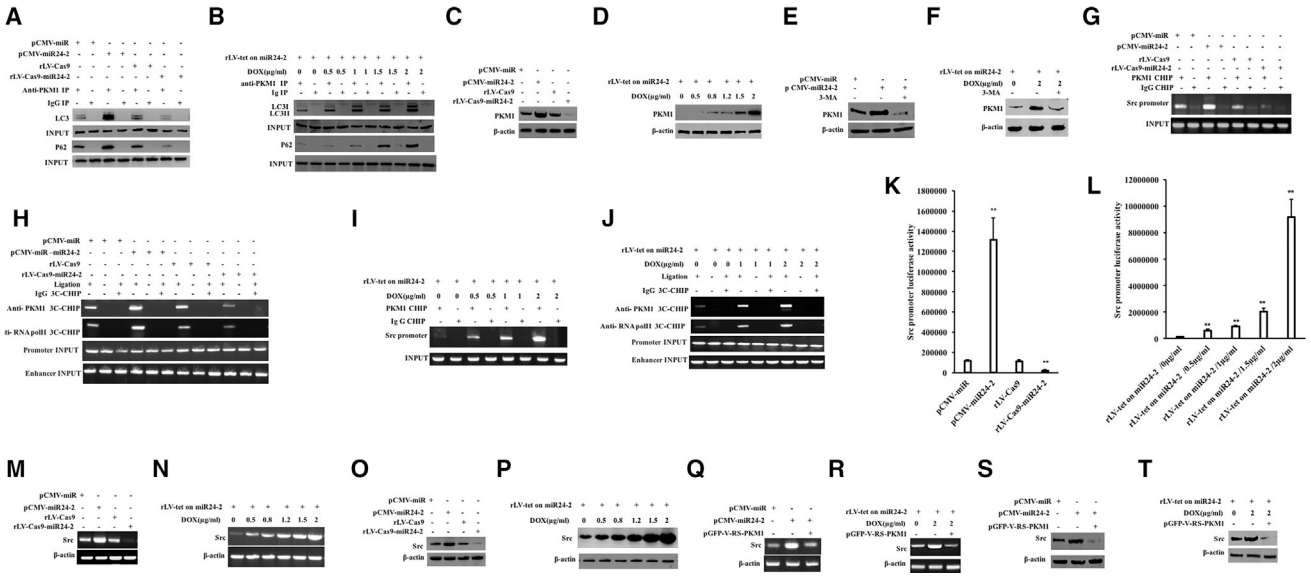

Figure 7. miR24-2 Promotes the Expression of the Tyrosine Protein Kinase Sarcoma Gene Src by Enhancing PKM1 in hLCSCs

(A) The coIP with anti-PKM1 was performed and the precipitates were analyzed by western blotting with anti-LC3 or anti-P62. IgG coIP was used as a negative control. (B) The coIP with anti-PKM1. (C) Western blotting using anti-PKM1. (D) Western blotting with anti-PKM1was performed. β-actin as an internal reference gene. (E) The total protein was subjected to western blotting using anti-PKM1. (F) Western blotting was performed using anti-PKM1. β-actin was used as an internal reference gene. (G) ChIP was performed using anti-PKM1. IgG ChIP was used as a negative control. (H) The binding ability of PKM1 to the Src promoter-enhancer loop was analyzed by chromosomal conformation capture (3C)-ChIP. IgG ChIP-3C was used as a negative control and the products amplified by independent primers designed by Src promoter and enhancer were used as internal reference (INPUT). (I) ChIP was performed. (J) 3C-ChIP was performed. (K) The pGL4-Src-Luc luciferase reporter activity was detected. (L) The pGL4-Src-Luc luciferase reporter gene activity was detected. (M) RT-PCR was used to detect Src. β-actin was used as an internal reference gene. (N) RT-PCR was used to detect Src. β-actin was used as an internal reference gene. (O) Western blotting was performed using anti-Src. (P) Western blotting was performed using anti-Src. (Q) RT-PCR was used to detect Src. (R) RT-PCR was used to detect Src. β-actin was used as an internal reference gene. (S) Western blotting was performed using anti-Src. (T) Western blotting was performed using anti-Src. β-actin was used as an internal reference gene.

Therefore, the expression of *Src* was significantly increased in the pCMV-miR24-2 group compared to the pCMV-miR group and reduced in the rLV-Cas9-miR24-2 group compared to the rLV-Cas9 group (Figures 7M and 7O). Moreover, the expression of *Src* was increased significantly as the increasing concentration of DOX in DOX (0 μg/mL) group, DOX (0.5 μg/mL) group, DOX (0.8 μg/mL) group, DOX (1.2 μg/mL) group, DOX (1.5 μg/mL) group, and DOX (2 μg/mL) group (Figures 7N and 7P). Moreover, the expression of Src was significantly increased in the pCMV-miR24-2 groups compared to the pCMV-miR group. However, there was no significant change between the pCMV-miR24-2+pGFP-V-RS-PKM1 group and pCMV-miR (Figures 7Q and 7S). Although the expression of *Src* was significantly increased in the DOX (2 μg/mL) group compared to the DOX (0 μg/mL) group, there was no significant change between the rLV-tet on-miR24-2/DOX (2 μg/mL) +pGFP-V-RS-PKM1 group compared to the DOX (0 μg/mL) group (Figures 7R and 7T). Collectively, these observations suggest that miR24-2 promotes the expression of *Src* through enhancing PKM1 in hLCSCs.

The Oncogenic Functions of miR24-2 Were Regulated by Src in Liver Cancer Stem Cells

To investigate whether the *Src* plays an important role in the malignant growth of hLCSCs triggered by miR24-2, hLCSCs were transfected with pCMV-miR, pCMV-miR24-2, and pCMV-miR24-2+pGFP-V-RS-Src, respectively. The excessive miR24-2 was produced in the pCMV-miR24-2 group and the pCMV-miR24-2+pGFP-V-RS-Src group (Figures 8A and 8B). And the expression of *Src* was significantly increased in the pCMV-miR24-2 group compared with the pCMV-miR group and reduced in the pCMV-miR24-2+pGFP-V-RS-Src group (Figure 8C). The proliferation ability of hLCSC was significantly increased in the pCMV-miR24-2 group compared with the pCMV-miR group ($p < 0.01$); however, there was no significant change between the pCMV-miR24-2+pGFP-V-RS-Src group and pCMV-miR group ($p > 0.05$) (Figure 8D). The BrdU-positive rate was significantly increased in the pCMV-miR24-2 group compared with the pCMV-miR group (34.91% ± 3.86% versus 70.15% ± 12.11%, $p = 0.0089263$). However, there was no significant change between the pCMV-miR24-2+pGFP-V-RS-Src group and pCMV-miR group (34.91% ± 3.86% versus 31.08% ± 2.503%, $p = 0.3234176$) (Figure 8E). The colony formation rate was significantly increased in the pCMV-miR24-2 group compared with the pCMV-miR group (37.24% ± 3.22% versus 37.24% ± 3.22%, $p = 0.0080199$). However, there was no significant change between the pCMV-miR24-2+pGFP-V-RS-Src group and pCMV-miR group (37.24% ± 3.22% versus 31.63% ± 8.72%, $p = 0.109668$) (Figure 8F). The sphere formation rate was significantly increased in

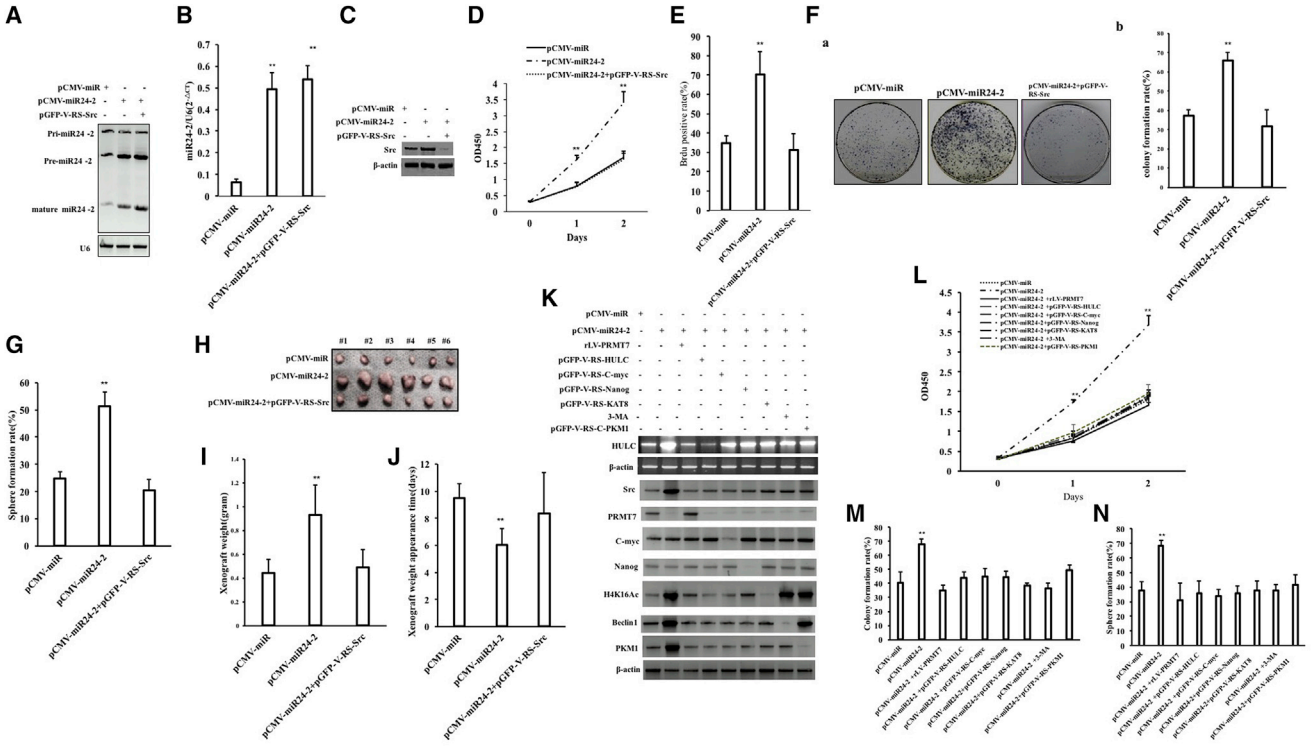

Figure 8. *Src* Affects miR24-2-Induced Malignant Growth of hLCSCs

(A) The miR24-2 was detected by northern blot. U6 was used as an internal reference gene. (B) The miR24-2 was detected by RT-PCR. (C) Western blotting was used to detect the Src. β-actin as an internal reference gene. (D) The cell proliferation ability was determined by the CCK8 method. (E) Determination of the S phase percentage of hLCSCs cells by BrdU staining. (F) Determination of plate colony forming ability of cells. (a) Photograph of plate colonies. (b) The analysis of cell plate colony formation rate. (G) The assay of cell sphere formation ability. (H) The hLCSCs were inoculated into the BALB/c nude mice for 1 month. Photography of xenografts. (I) Comparison of the size (g) of transplanted tumors in nude mice (n = 6). $^{**}p < 0.01$, $^{*}p < 0.05$. (J) The comparison of appearance time (days) of transplanted tumors in nude mice (n = 6). $^{**}p < 0.01$, $^{*}p < 0.05$. (K) RT-PCR was used to detect HULC, and western blotting was used to detect the expression of Src, PRMT7, C-myc, Nanog, Beclin1, H4K16Ac, and PKM1. β-actin was used as an internal reference gene. (L) The cell proliferation ability was determined by the CCK8 method. (M) The analysis of cell plate colony formation rate. (N) The assay of cell sphere formation ability. $^{**}p < 0.01$, $^{*}p < 0.05$.

the pCMV-miR24-2 group compared with the pCMV-miR group (24.68% ± 2.68% versus 51.41% ± 5.31%, p = 0.00998). However, there was no significant change between the pCMV-miR24-2+pGFP-V-RS-Src group and pCMV-miR group (24.68% ± 2.68% versus 20.31% ± 4.23%, p = 0.0515) (Figure 8G). Although the average weight of transplanted tumors was significantly increased in the pCMV-miR24-2 group compared with the pCMV-miR group (0.44 ± 0.12 g versus 0.93 ± 0.25 g, p = 0.0015983), there was no significant change between the pCMV-miR24-2+pGFP-V-RS-Src group and pCMV-miR group (0.44 ± 0.12 g versus 0.49 ± 0.15 g, p = 0.1487) (Figures 8H and 8I). And the average appearance time of transplanted tumors was significantly reduced in the pCMV-miR24-2 group compared with the pCMV-miRs group (9.5 ± 1.05 days versus 6 ± 1.26 days, p = 0.0017085). However, there was no significant change between the pCMV-miR24-2+pGFP-V-RS-Src group and pCMV-miR group (9.5 ± 1.05 days versus 8.83 ± 3.06 days, p = 0.3475961) (Figure 8J). Although the poorly differentiated tumor cells were significantly increased in the pCMV-miR24-2 group compared with the pCMV-miR group, there was no significant change between the pCMV-miR24-2+pGFP-V-RS-Src group and pCMV-miR group (Figure S12). Notably, although the expression of *Src*, the cell proliferation ability, colony formation rate, and sphere formation rate were significantly increased in the pCMV-miR24-2 group compared with the pCMV-miR group, there was no significant change in the pCMV-miR24-2+pGFP-V-RS-HULC group, pCMV-miR24-2+rLV-PRMT7 group, pCMV-miR24-2+pGFP-V-RS-C-myc group, pCMV-miR24-2+pGFP-V-RS-Nanog group, pCMV-miR24-2+3-MA group, pCMV-miR24-2+pGFP-V-KAT8 group, and pCMV-miR24-2+pGFP-V-RS-PKM1 group compared to pCMV-miR group, respectively (Figures 8K–8N). Collectively, these results suggest that Src regulates and controls the oncogenic functions of miR24-2 in hLCSCs positively.

DISCUSSION

At the present, we clearly demonstrate that miR24-2 enhances the expression and function of the tyrosine protein kinase sarcoma gene *Src* in LCSCs and promotes the malignant growth of LCSCs (Figure S13). In this study, it was confirmed that miR24-2 is a microRNA

with cancerous function, which is shown at least in human liver cancer. Moreover, Nanog, HDAC3, and PI3K are key players in this signaling pathway mediated by miR24-2 specifically.

Studies have reported that miR24-2 is involved in tumorigenesis. For example, miRNA24-2 promotes the development of tumors such as gastric cancer and breast cancer by enhancing the expression of oncogenes such as c-Myc.[24,25] However, there are some reports that miR24-2 negatively regulates the growth of tumor cells. For example, miR24-2 can regulate different apoptotic pathways and induce apoptosis.[16,26] Therefore, we believe that miR24-2 is likely to play a specific role through different mechanisms in different tumor cells and its corresponding environments.

It is well known that epigenetic modifications mainly include histone modifications and nucleic acid modifications, which play an important role in the regulation of gene expression, and epigenetic disorders are common features of most cancers.[27] Our findings suggest that miR24-2 alters the expression of various histone H3/4 epigenetic modifications, indicating that miR24-2 can play a regulatory role in the development of liver cancer epigenetically. Our findings suggest that miR24-2 inhibits the expression of *PRMT7*. It was reported that PRMT7 can promote methylation of arginine at position 3 of histone H4[28] and inhibits the expression of certain genes by upregulating the symmetrical dimethylation level of H4R3.[17,29,30] We demonstrate that miR24-2 can target PRMT7 and reduce the bi/trimethylation of histone H4R3 and then miR24-2 causes the changes in the function of some important genes, such as HULC, in liver cancer cells. Notably, studies have also reported that H4R3me2 is a marker of transcriptional repression.[31]

Furthermore, miR24-2-dependent miR675 inhibits the expression of histone deacetylase HDAC3, which plays an important role in the regulation of histone modification and is generally considered to be a locus-specific co-suppressor, which is recruited to the promoter.[32,33] Moreover, miR24-2 increased the H4K16Ac modification by inhibiting the expression of HDAC3, which in turn altered the expression of certain genes. Surprisingly, miR24-2 also triggers a change in the methylation level of histone H4 lysine 20 (H4K20) and histone H3 lysine 79 (H3K79). Methylation of H4K20 plays a key role in regulating high-level chromosome structure and X chromosome gene expression,[34] and H3K79me2 is a histone marker associated with transcriptional active genes.[35] In this study, the methylation levels of H4K20 and H3K79 did not change after knockdown of H4K16Ac-specific acetyltransferase KAT8 in miR24-2 overexpressing cells. It was shown that miR24-2 altered the methylation modification of H4K20 and H3K79 dependent on H4K16Ac. Importantly, these changes in epigenetic modifications further cause altering of certain genes, such as PI3K.

Notably, our findings indicate that miR24-2 can play a carcinogenic role together with other noncoding RNAs including miRNA and long noncoding RNAs (lncRNAs) such as miR675, HULC, etc. This study found that miR24-2 could increase the transcriptional activity and maturation of pri-miR675 by promoting the binding of Nanog to the miR675 precursor (pri-miR675) promoter in hLCSCs. miR675 plays a different role in tumors, and this inhibits DNA damage repair and regulates abnormal expression of cell-cycle-related genes.[36–38] Although miR24-2 may play a carcinogenic role through miR675, its detailed mechanism needs further to be confirmed. Importantly, our results identify that miR24-2 can increase the transcriptional activity of HULC by inhibiting the modification of H4R3me2/3 to the HULC promoter region. HULC is dysregulated in many types of cancer and promotes proliferation, invasion, migration, and angiogenesis of cancer cells.[20,39,40] Our study indicates that miR24-2 enhances the binding of HULC to some molecules, such as KLF4, c-Myc, Epcam, etc., which enhances the expression of Nanog and promotes autophagy through downstream signaling pathway. It can be seen that lncRNA HULC plays a key role in the carcinogenesis triggered by miR24-2.

Strikingly, our results demonstrate that the function of miR24-2 is related to autophagy in hLCSCs. First, miR24-2 increases the expression and lipidation of the autophagy structural protein LC3 in hLCSCs. During autophagy, LC3 (LC3-I) in the cytoplasm combines with phosphatidylethanolamine to form LC3-phosphatidylethanolamine conjugate (LC3-II), which is recruited to the autophagosome membrane. Therefore, the autophagosome marker LC3-II reflects autophagy activity.[41,42] In this study, miR24-2 promotes the expression of LC3 and the formation of LC3-II, indicating that miR24-2 is involved in the regulation of autophagy and promotes the production of autophagy. Second, miR24-2 enhances the interaction between LC3 and the LC3 cleavage protein ATG4 in hLCSCs. Studies have shown that ATG4 is essential for autophagy and highly specific.[43] During autophagy, LC3 undergoes two steps, namely proteolytic cleavage of LC3 and delipidation of LC3-PE in autophagosomes, both catalyzed by ATG4.[44] This study suggests that miR24-2 enhances the function of ATG4, leads to the cleavage of LC3, and further forms activated LC3II, which is a key step in the process of autophagy, further indicating that miR24-2 is involved in the regulation of autophagy. Third, miR24-2 increases the interaction of LC3II with the activated LC3II processing protein ATG3. ATG3 is an E2-like enzyme required for LC3 lipidation during autophagy.[45] When autophagy occurs, ATG3 binds to LC3 and lipidation of LC3 occurs, a process that is the initial step in autophagy. Thus, this study suggests that miR24-2 may affect the initiation of autophagy through the binding of ATG3 to LC3II. Fourthly, miR24-2 increased the expression of the autophagy marker protein Beclin1, indicating that miR24-2 promotes autophagy in hLCSCs. It is reported that Beclin1 is a coiled-coil protein that interacts with Bcl-2 and promotes autophagy.[46] In this study, the expression of Beclin1 was elevated in hLCSCs overexpressing miR24-2, further confirming that miR24-2 regulates the expression of Beclin1 to promote autophagy. Finally, miR24-2 enhances PI3K expression by altering histone modifications such as H4K16Ac, H4K20me2/3, etc. PI3K plays an important role in autophagy, membrane trafficking, and cell signaling[47] and interacts with Beclin1 to participate in autophagy.[48,49] In this study, after knocking down PI3K in miR24-2 overexpressing hLCSCs, the function of miR24-2

to promote autophagy was fully abolished, indicating that miR24-2-dependent PI3K promotes autophagy.

It is worth noting that protein kinases can be involved in most of the signal transduction in eukaryotic cells and regulate many cellular processes.[50,51] In this study, miR24-2 affected the expression and function of several protein kinases, including PKM1, and Src, indicating that miR24-2 exerts its carcinogenic function at least in part by altering protein kinase activity in hLCSCs. PKM1 is a protein kinase that activates glucose catabolism and stimulates autophagy, thereby enhancing the malignant growth of tumor cells.[52] miR24-2-dependent autophagy enhanced the expression and function of PKM1 in hLCSCs, indicating that PKM1 plays an important role in the carcinogenic functions of miR24-2. Furthermore, the function of miR24-2 is associated with the tyrosine protein kinase sarcoma gene *Src*. Studies have shown that the Src kinase family is a class of non-receptor tyrosine kinases.[53] In particular, Src plays a key role in tumor development and is involved in the regulation of proliferation, survival, migration, invasion, and metastasis of various tumor cells.[54] In this study, miR24-2-dependent PKM1 promotes the expression of Src, and knockdown of *Src* substantially abolishes the tumorigenic ability of miR24-2, indicating that Src may decide the oncogenic action of miR24-2 at least in LCSCs.

So far, our study clearly reveals some of the mechanisms by which miR24-2 plays a carcinogenic role in human LCSCs, but the detailed mechanisms of specific processes remain to be further studied. These interesting findings will provide a valuable theoretical basis for the discovery of liver cancer therapeutic targets and diagnosis markers based on miR-24-2.

MATERIALS AND METHODS

Bioinformatics Analysis

Bioinformatics analysis was performed by MirTarget scanning software, RNA22 software, BLAST tools, miRanda, RNA hybrid and PicTar, and TCGA miRNA expression profile.

hLCSC Sorting

CD133/CD44/CD24/EpCAM MicroBead Kits were purchased from Miltenyi Biotec (Boston, USA) and MACS Technology and performed the operation according to the manufacturer.

Cell Lines, Lentivirus, and Plasmids

hLCSCs were maintained in DMEM (GIBCO BRL Life Technologies) supplemented with 10% fetal bovine serum (Sigma) in a humidified atmosphere of 5% CO_2 incubator at 37°C. rLV were purchased from Wu Han viraltherapy Technologies. pCMV-miR was purchased from Origene (Rockville, MD, USA).

RT-PCR

Total RNA was purified using Trizol (Invitrogen) according to the manufacturer's instructions. cDNA was prepared by SuperScript First-Strand Synthesis System (Invitrogen). PCR analysis was performed according to the manufacturer's instructions.

Western Blotting

The samples containing cellular proteins were separated on a 10% SDS-PAGE and transferred onto a nitrocellulose membrane (Amersham). The blots were incubated with antibody at 4°C overnight. Following three washes, membranes were then incubated with secondary antibody at 4°C overnight. Signals were visualized by ECL System (Amersham).

CoIP

Cells were lysed in the whole-cell extract buffer A (50 mM pH 7.6 Tris-HCl, 150 mM NaCl, 1% NP40, 0.1mM EDTA,1.0 mM DTT,0.2 mM PMSF, 0.1 mM Pepstatine,0.1 mM Leupeptine, 0.1 mM Aproine). 500 μL of cell lysates was used in immunoprecipitation with antibody. Western blot was performed with another related antibody.

RNA Immunoprecipitation

Ribonucleoprotein particle-enriched lysates were incubated with protein A/G-plus agarose beads (Santa Cruz, Biotechnology, CA) together with specific antibody for 4 hours at 4°C. Beads were subsequently washed four times with 50 mM Tris-HCl (pH 7.0), 150 mM NaCl, 1 mM $MgCl_2$, and 0.05% NP-40, and twice after addition of 1 M urea. mRNAs were then isolated and purified for RT-PCR according to the manufacturer's instructions.

Chromosome Conformation Capture-ChIP

Chromatin bound to the antibody-protein-A/G-Sepharose beads were resuspended and the ChIP-chromosome conformation capture (3C) material was detected for long-range interaction with specific primers according to the manufacturer's instructions.

Super-EMSA (Gel-Shift)

Cells were washed and scraped in ice-cold PBS to prepare nuclei for electrophoretic gel mobility shift assay with the use of the gel shift assay system modified according to the manufacturer's instructions.

Cells Proliferation CCK8 Assay

The cell proliferation reagent CCK8 was purchased from Roche and the operation was performed according to the manufacturer's instruction.

Colony-Formation Efficiency Assay

Cells were plated on a six-well plate and the DMEM containing 10% FBS was added into each well of the three replicates. Cell colonies were stained with Crystal Violet.

Xenograft Transplantation *In Vivo*

The male athymic BALB/c mice were injected with hLCSCs at the armpit area subcutaneously. The mice were observed for 4 weeks and then sacrificed to recover the tumors. The use of mice for this work was reviewed and approved by the institutional animal care and use committee in accordance with China National Institutes of Health guidelines.

SUPPLEMENTAL INFORMATION

Supplemental Information can be found online at https://doi.org/10.1016/j.ymthe.2019.10.015.

AUTHOR CONTRIBUTIONS

D.L. conceived the study and participated in the study design, performance, coordination, and manuscript writing. L.W., X.L., W.Z., Y.Y., Q.M., C.W., X.X., X.J., S.S., Y.L., H.P., X.G.,T.L., J.X., J.L., and S.J. performed the research. All authors have read and approved the final manuscript.

CONFLICTS OF INTEREST

The authors declare no competing interests.

ACKNOWLEDGMENTS

This study was supported by grants from the National Natural Science Foundation of China (NCSF grant numbers 81572773 and 81773158) and by a grant from the Science and Technology Commission of Shanghai Municipality Basic Research Field Project (19JC1415200).

REFERENCES

1. Visvader, J.E., and Lindeman, G.J. (2008). Cancer stem cells in solid tumours: accumulating evidence and unresolved questions. Nat. Rev. Cancer *8*, 755–768.
2. Rosental, B., Kowarsky, M., Seita, J., Corey, D.M., Ishizuka, K.J., Palmeri, K.J., Chen, S.Y., Sinha, R., Okamoto, J., Mantalas, G., et al. (2018). Complex mammalian-like haematopoietic system found in a colonial chordate. Nature *564*, 425–429.
3. Messal, H.A., Alt, S., Ferreira, R.M.M., Gribben, C., Wang, V.M., Cotoi, C.G., Salbreux, G., and Behrens, A. (2019). Tissue curvature and apicobasal mechanical tension imbalance instruct cancer morphogenesis. Nature *566*, 126–130.
4. Sánchez-Danés, A., Larsimont, J.C., Liagre, M., Muñoz-Couselo, E., Lapouge, G., Brisebarre, A., Dubois, C., Suppa, M., Sukumaran, V., del Marmol, V., et al. (2018). A slow-cycling LGR5 tumour population mediates basal cell carcinoma relapse after therapy. Nature *562*, 434–438.
5. Choe, J., Lin, S., Zhang, W., Liu, Q., Wang, L., Ramirez-Moya, J., Du, P., Kim, W., Tang, S., Sliz, P., et al. (2018). mRNA circularization by METTL3-eIF3h enhances translation and promotes oncogenesis. Nature *561*, 556–560.
6. Ma, S., Chan, K.W., Hu, L., Lee, T.K., Wo, J.Y., Ng, I.O., Zheng, B.J., and Guan, X.Y. (2007). Identification and characterization of tumorigenic liver cancer stem/progenitor cells. Gastroenterology *132*, 2542–2556.
7. Yang, Z.F., Ho, D.W., Ng, M.N., Lau, C.K., Yu, W.C., Ngai, P., Chu, P.W., Lam, C.T., Poon, R.T., and Fan, S.T. (2008). Significance of CD90+ cancer stem cells in human liver cancer. Cancer Cell *13*, 153–166.
8. Lui, S.K., Vilchez, V., and Gedaly, R. (2015). Liver Cancer Stem Cells: A New Paradigm for Hepatocellular Carcinoma Treatment. J. Stem Cell Res. Ther. *5*, 283.
9. Wang, D., Si, S., Wang, Q., Luo, G., Du, Q., Liang, Q., Guo, X., Zhang, G., Feng, J., and Leng, Z. (2018). MiR-27a Promotes Hemin-Induced Erythroid Differentiation of K562 Cells by Targeting CDC25B. Cell. Physiol. Biochem. *46*, 365–374.
10. Wang, Y., Zhang, Y., Su, X., Wang, H., Yang, W., and Zan, L. (2018). Cooperative and Independent Functions of the *miR-23a∼27a∼24-2* Cluster in Bovine Adipocyte Adipogenesis. Int. J. Mol. Sci. *19*, E3957.
11. Teteloshvili, N., Dekkema, G., Boots, A.M., Heeringa, P., Jellema, P., de Jong, D., Terpstra, M., Brouwer, E., Pawelec, G., Kok, K., et al. (2018). Involvement of MicroRNAs in the Aging-Related Decline of CD28 Expression by Human T Cells. Front. Immunol. *9*, 1400.
12. Zeng, H.C., Bae, Y., Dawson, B.C., Chen, Y., Bertin, T., Munivez, E., Campeau, P.M., Tao, J., Chen, R., and Lee, B.H. (2017). MicroRNA miR-23a cluster promotes osteocyte differentiation by regulating TGF-β signalling in osteoblasts. Nat. Commun. *8*, 15000.
13. Cheng, A.M., Byrom, M.W., Shelton, J., and Ford, L.P. (2005). Antisense inhibition of human miRNAs and indications for an involvement of miRNA in cell growth and apoptosis. Nucleic Acids Res. *33*, 1290–1297.
14. Martin, E.C., Elliott, S., Rhodes, L.V., Antoon, J.W., Fewell, C., Zhu, Y., Driver, J.L., Jodari-Karimi, M., Taylor, C.W., Flemington, E.K., et al. (2014). Preferential star strand biogenesis of pre-miR-24-2 targets PKC-alpha and suppresses cell survival in MCF-7 breast cancer cells. Mol. Carcinog. *53*, 38–48.
15. Manvati, S., Mangalhara, K.C., Kalaiarasan, P., Srivastava, N., and Bamezai, R.N. (2015). miR-24-2 regulates genes in survival pathway and demonstrates potential in reducing cellular viability in combination with docetaxel. Gene *567*, 217–224.
16. Li, X., Liu, X., Xu, W., Zhou, P., Gao, P., Jiang, S., Lobie, P.E., and Zhu, T. (2013). c-MYC-regulated miR-23a/24-2/27a cluster promotes mammary carcinoma cell invasion and hepatic metastasis by targeting Sprouty2. J. Biol. Chem. *288*, 18121–18133.
17. Lee, S.H., Chen, T.Y., Dhar, S.S., Gu, B., Chen, K., Kim, Y.Z., Li, W., and Lee, M.G. (2016). A feedback loop comprising PRMT7 and miR-24-2 interplays with Oct4, Nanog, Klf4 and c-Myc to regulate stemness. Nucleic Acids Res. *44*, 10603–10618.
18. Musto, A., Navarra, A., Vocca, A., Gargiulo, A., Minopoli, G., Romano, S., Romano, M.F., Russo, T., and Parisi, S. (2015). miR-23a, miR-24 and miR-27a protect differentiating ESCs from BMP4-induced apoptosis. Cell Death Differ. *22*, 1047–1057.
19. Keniry, A., Oxley, D., Monnier, P., Kyba, M., Dandolo, L., Smits, G., and Reik, W. (2012). The H19 lincRNA is a developmental reservoir of miR-675 that suppresses growth and Igf1r. Nat. Cell Biol. *14*, 659–665.
20. He, D., Wang, J., Zhang, C., Shan, B., Deng, X., Li, B., Zhou, Y., Chen, W., Hong, J., Gao, Y., et al. (2015). Down-regulation of miR-675-5p contributes to tumor progression and development by targeting pro-tumorigenic GPR55 in non-small cell lung cancer. Mol. Cancer *14*, 73.
21. Panzitt, K., Tschernatsch, M.M., Guelly, C., Moustafa, T., Stradner, M., Strohmaier, H.M., Buck, C.R., Denk, H., Schroeder, R., Trauner, M., and Zatloukal, K. (2007). Characterization of HULC, a novel gene with striking up-regulation in hepatocellular carcinoma, as noncoding RNA. Gastroenterology *132*, 330–342.
22. Yao, R., Jiang, H., Ma, Y., Wang, L., Wang, L., Du, J., Hou, P., Gao, Y., Zhao, L., Wang, G., et al. (2014). PRMT7 induces epithelial-to-mesenchymal transition and promotes metastasis in breast cancer. Cancer Res. *74*, 5656–5667.
23. Jain, K., Jin, C.Y., and Clarke, S.G. (2017). Epigenetic control via allosteric regulation of mammalian protein arginine methyltransferases. Proc. Natl. Acad. Sci. USA *114*, 10101–10106.
24. Hua, K., Chen, Y.T., Chen, C.F., Tang, Y.S., Huang, T.T., Lin, Y.C., Yeh, T.S., Huang, K.H., Lee, H.C., Hsu, M.T., et al. (2018). MicroRNA-23a/27a/24-2 cluster promotes gastric cancer cell proliferation synergistically. Oncol. Lett. *16*, 2319–2325.
25. He, H.W., Wang, N.N., Yi, X.M., Tang, C.P., and Wang, D. (2018). Low-level serum miR-24-2 is associated with the progression of colorectal cancer. Cancer Biomark. *21*, 261–267.
26. Srivastava, N., Manvati, S., Srivastava, A., Pal, R., Kalaiarasan, P., Chattopadhyay, S., Gochhait, S., Dua, R., and Bamezai, R.N. (2011). miR-24-2 controls H2AFX expression regardless of gene copy number alteration and induces apoptosis by targeting antiapoptotic gene BCL-2: a potential for therapeutic intervention. Breast Cancer Res. *13*, R39.
27. Mohammad, H.P., Barbash, O., and Creasy, C.L. (2019). Targeting epigenetic modifications in cancer therapy: erasing the roadmap to cancer. Nat. Med. *25*, 403–418.
28. Jelinic, P., Stehle, J.C., and Shaw, P. (2006). The testis-specific factor CTCFL cooperates with the protein methyltransferase PRMT7 in H19 imprinting control region methylation. PLoS Biol. *4*, e355.
29. Jain, K., and Clarke, S.G. (2019). PRMT7 as a unique member of the protein arginine methyltransferase family: A review. Arch. Biochem. Biophys. *665*, 36–45.
30. Chang, B., Chen, Y., Zhao, Y., and Bruick, R.K. (2007). JMJD6 is a histone arginine demethylase. Science *318*, 444–447.
31. Dhar, S.S., Lee, S.H., Kan, P.Y., Voigt, P., Ma, L., Shi, X., Reinberg, D., and Lee, M.G. (2012). Trans-tail regulation of MLL4-catalyzed H3K4 methylation by H4R3 symmetric dimethylation is mediated by a tandem PHD of MLL4. Genes Dev. *26*, 2749–2762.

32. Jones, P.L., and Shi, Y.B. (2003). N-CoR-HDAC corepressor complexes: roles in transcriptional regulation by nuclear hormone receptors. Curr. Top. Microbiol. Immunol. *274*, 237–268.

33. Bhaskara, S., Knutson, S.K., Jiang, G., Chandrasekharan, M.B., Wilson, A.J., Zheng, S., Yenamandra, A., Locke, K., Yuan, J.L., Bonine-Summers, A.R., et al. (2010). Hdac3 is essential for the maintenance of chromatin structure and genome stability. Cancer Cell *18*, 436–447.

34. Brejc, K., Bian, Q., Uzawa, S., Wheeler, B.S., Anderson, E.C., King, D.S., Kranzusch, P.J., Preston, C.G., and Meyer, B.J. (2017). Dynamic Control of X Chromosome Conformation and Repression by a Histone H4K20 Demethylase. Cell *171*, 85–102.e23.

35. Bernt, K.M., Zhu, N., Sinha, A.U., Vempati, S., Faber, J., Krivtsov, A.V., Feng, Z., Punt, N., Daigle, A., Bullinger, L., et al. (2011). MLL-rearranged leukemia is dependent on aberrant H3K79 methylation by DOT1L. Cancer Cell *20*, 66–78.

36. Lu, Y., Song, S., Jiang, X., Meng, Q., Wang, C., Li, X., Yang, Y., Xin, X., Zheng, Q., Wang, L., et al. (2019). miR675 Accelerates Malignant Transformation of Mesenchymal Stem Cells by Blocking DNA Mismatch Repair. Mol. Ther. Nucleic Acids *14*, 171–183.

37. Tsang, W.P., Ng, E.K., Ng, S.S., Jin, H., Yu, J., Sung, J.J., and Kwok, T.T. (2010). Oncofetal H19-derived miR-675 regulates tumor suppressor RB in human colorectal cancer. Carcinogenesis *31*, 350–358.

38. Yang, Y., Meng, Q., Wang, C., Li, X., Lu, Y., Xin, X., Zheng, Q., and Lu, D. (2018). MicroRNA 675 cooperates PKM2 to aggravate progression of human liver cancer stem cells induced from embryonic stem cells. J. Mol. Med. (Berl.) *96*, 1119–1130.

39. Chen, S., Wu, D.D., Sang, X.B., Wang, L.L., Zong, Z.H., Sun, K.X., Liu, B.L., and Zhao, Y. (2017). The lncRNA HULC functions as an oncogene by targeting ATG7 and ITGB1 in epithelial ovarian carcinoma. Cell Death Dis. *8*, e3118.

40. Li, D., Liu, X., Zhou, J., Hu, J., Zhang, D., Liu, J., Qiao, Y., and Zhan, Q. (2017). Long noncoding RNA HULC modulates the phosphorylation of YB-1 through serving as a scaffold of extracellular signal-regulated kinase and YB-1 to enhance hepatocarcinogenesis. Hepatology *65*, 1612–1627.

41. Levy, J.M.M., Towers, C.G., and Thorburn, A. (2017). Targeting autophagy in cancer. Nat. Rev. Cancer *17*, 528–542.

42. Tanida, I., Ueno, T., and Kominami, E. (2008). LC3 and Autophagy. Methods Mol. Biol. *445*, 77–88.

43. Maruyama, T., and Noda, N.N. (2017). Autophagy-regulating protease Atg4: structure, function, regulation and inhibition. J. Antibiot. (Tokyo) *71*, 72–78.

44. Pengo, N., Agrotis, A., Prak, K., Jones, J., and Ketteler, R. (2017). A reversible phospho-switch mediated by ULK1 regulates the activity of autophagy protease ATG4B. Nat. Commun. *8*, 294.

45. Radoshevich, L., Murrow, L., Chen, N., Fernandez, E., Roy, S., Fung, C., and Debnath, J. (2010). ATG12 conjugation to ATG3 regulates mitochondrial homeostasis and cell death. Cell *142*, 590–600.

46. Liang, X.H., Jackson, S., Seaman, M., Brown, K., Kempkes, B., Hibshoosh, H., and Levine, B. (1999). Induction of autophagy and inhibition of tumorigenesis by beclin 1. Nature *402*, 672–676.

47. Miller, S., Tavshanjian, B., Oleksy, A., Perisic, O., Houseman, B.T., Shokat, K.M., and Williams, R.L. (2010). Shaping development of autophagy inhibitors with the structure of the lipid kinase Vps34. Science *327*, 1638–1642.

48. He, C., Wei, Y., Sun, K., Li, B., Dong, X., Zou, Z., Liu, Y., Kinch, L.N., Khan, S., Sinha, S., et al. (2013). Beclin 2 functions in autophagy, degradation of G protein-coupled receptors, and metabolism. Cell *154*, 1085–1099.

49. Shelly, S., Lukinova, N., Bambina, S., Berman, A., and Cherry, S. (2009). Autophagy is an essential component of Drosophila immunity against vesicular stomatitis virus. Immunity *30*, 588–598.

50. Manning, G., Whyte, D.B., Martinez, R., Hunter, T., and Sudarsanam, S. (2002). The protein kinase complement of the human genome. Science *298*, 1912–1934.

51. Leopold, A.V., Chernov, K.G., and Verkhusha, V.V. (2018). Optogenetically controlled protein kinases for regulation of cellular signaling. Chem. Soc. Rev. *47*, 2454–2484.

52. Morita, M., Sato, T., Nomura, M., Sakamoto, Y., Inoue, Y., Tanaka, R., Ito, S., Kurosawa, K., Yamaguchi, K., Sugiura, Y., et al. (2018). PKM1 Confers Metabolic Advantages and Promotes Cell-Autonomous Tumor Cell Growth. Cancer Cell *33*, 355–367.e7.

53. Ishizawar, R., and Parsons, S.J. (2004). c-Src and cooperating partners in human cancer. Cancer Cell *6*, 209–214.

54. Zhang, S., and Yu, D. (2012). Targeting Src family kinases in anti-cancer therapies: turning promise into triumph. Trends Pharmacol. Sci. *33*, 122–128.

YMTHE, Volume *28*

Supplemental Information

miR24-2 Promotes Malignant Progression of Human Liver Cancer Stem Cells by Enhancing Tyrosine Kinase Src Epigenetically

Liyan Wang, Xiaonan Li, Wei Zhang, Yuxin Yang, Qiuyu Meng, Chen Wang, Xiaoru Xin, Xiaoxue Jiang, Shuting Song, Yanan Lu, Hu Pu, Xin Gui, Tianming Li, Jie Xu, Jiao Li, Song Jia, and Dongdong Lu

Supplemental Materials and Methods

Expression plasmid for human miR24-2

Human miR24-2 expression plasmidwas purchased from Origene (CAT#: SC400297). pCMV-miR vector for miRNA expression clone with GFP as reporter expresses microRNA precursors from CMV promoter. The miR24-2 precursor insert was cloned between SgfI and MluI site and Neomycin selection marker for stable cell establishment.

rLV-U6 -miR24-2 sgRNA-Cas9-ZsGreen Lentiviral

Both the vector plasmid pLVX-U6-Cas9-ZsGreen (Wuhan Venuosai Biotechnology Co., Ltd.) and the target gene plasmid pUC57-hsa-miR24-2 sgRNA (CTCTGCCT***CCCGTGCCTACTGAGCTGAA***ACACAGTTGGTTTGTGTACACTG GCTCAGTTCAGCAGGAACAGGG) were double-digested, and the large fragment of plasmid pLVX-U6-Cas9-ZsGreen and the small fragment of plasmid pUC57-has-miR24-2 sgRNA were recovered by 1% agarose gel electrophoresis. The two plasmid fragment was then carried out ligation reaction at 16 ° C for 4 hours, and the ligation product was transformed into JM109 competent bacterial and cultured

overnight. Monoclonal colonies were picked for sequencing verification. The recombinant plasmid pLVX-U6-miR24-2 sgRNA-Cas9-ZsGreen was transfected into 293 T cells to generate a high titer lentivirus containing the gene of interest (rLV-Cas9-miR24-2).

Tetracycline (DOX) inducting lentiviral rLV-tet on-miR24-2

The expression plasmid pLVX-tet on-Tight-EF1a-ZsGreen and the target gene plasmid pUC57-has-miR24-2 were digested with BamHI and NotI, respectively, and the large fragment of plasmid pLVX-tet on-Tight-EF1a -ZsGreen and the small fragment pUC57-miR24-2 were recovered by 1% agarose gel electrophoresis respectively. The two plasmid pLVX-tet on-Tight-EF1a-ZsGreen (BamHI+NotI) and pUC57-miR24-2 (BamHI+NotI) were carried out the ligation reaction at 22 ° C for 3 hours and then the ligation products were transformed t into JM109 competent bacterial overnight. Monoclonal colonies were picked for sequencing verification. The recombinant plasmid pLVX-tet on-miR24-2-Tight-EF1a-ZsGreen containing the

gene of interest was transfected into 293 T cells to generate a high titer lentivirus containing the gene of interest (rLV-tet on miR24-2).

Expression Lentivirus for human miR675

The vector plasmid pLVX-ZsGreen-miRNA-Puro (Wuhan Venuosai Biotechnology Co., Ltd.) and the target gene plasmid pUC57-has-miR675 (MI0005416) were double-digested with BamHI and NotI, respectively, and he large fragment of plasmid pLVX-ZsGreen-miRNA-Puro and the small fragment of plasmid pUC57-has-miR675 was recovered by 1% agarose gel electrophoresis. The two plasmid fragments were performed ligation reaction t at 22 ° C for 3 hours, and the ligation product was transformed into JM109 competent bacterial and cultured overnight. The monoclonal colonies were picked for sequencing verification, and the sequencing primer: ZsGreen-F (5'-GCGACGCCAAGAACCAGAAG-3'). The recombinant plasmid pLVX-ZsGreen-miR675-Puro containing the gene of interest was transfected into 293 T cells, respectively, generating a lentivirus containing a gene of interest at a high titer (rLV-miR675).

rLV-U6 –miR675 sgRNA-Cas9-ZsGreen Lentiviral

Both the vector plasmid pLVX-U6-Cas9-ZsGreen (Wuhan Venuosai Biotechnology Co., Ltd.) and the target gene plasmid pUC57-hsa-miR675 sgRNA (CTGTTAATGCTAATCGTGATAGGGGTTTTTGCCT*CACTGTGGGCCCTCTCC GCACCA*AGCATTAACAG) were double-digested, and the large fragment of plasmid pLVX-U6-Cas9-ZsGreen and the small fragment of plasmid pUC57-has-miR675 sgRNA were recovered by 1% agarose gel electrophoresis. The two plasmid fragment was then carried out ligation reaction at 16 ° C for 4 hours, and the ligation product was transformed into JM109 competent bacterial and cultured overnight. Monoclonal colonies were picked for sequencing verification. The recombinant plasmid pLVX-U6-miR675 sgRNA-Cas9-ZsGreen was transfected into 293 T cells to generate a high titer lentivirus containing the gene of interest (rLV-Cas9-miR675).

Northern-Western blotting for miRNA RNA samples were separated on 15% polyacrylamide/8M urea gel. Soak Hybond-N+ membrane (Amersham Pharmacia,

Uppsala, Sweden) in ddH2O for a few seconds and in transfer buffer (0.5X TBE) for 20 minutes ,and soak two pieces of whatman paper in 0.5XTBE . Separated RNA in gel was electro-blotted onto Hybond-N+ membrane (Amersham Pharmacia, Uppsala, Sweden). After UV cross-linking and air drying, blotted membrane was prehybridized with hybridization buffer at 42 ºC for 60 min, and then hybridized with Biotin-labeled antisense miR24-2 probe and incubated at 42 ºC for overnight. The membrane was washed 4 times at 42 ºC with 2x SSC and 0.5% SDS and then western blotting with anti-Biotin according to the our pervious protocol.

Supplemental Results

The isolation of human liver cancer cell (hLCSCs)

hLCSCs were isolated from human liver cancer cell line Huh7 using CD133/CD44/CD24/EpCAM microbeads(**Fig.S1A**). CD133, CD44, CD24 or EpCAM were positively expressed in hLCSCs and not expressed in non-hLCSCs (**Fig. S1B-D**).

The knockout of miR-24-2 did not affect the expression of miR-23a and miR-27a in liver cancer stem cells

We performed the Northern-Wstern blotting in rLV-Cas9 group and rLV-Cas9 –miR 24-2group and the results showed the there are no significant difference of miR-23a(250bp pri-miR-23a,73bp premiR23a, 22bp mature miR23a) between rLV-Cas9 group and rLV-Cas9 –miR24-2group(**FigureS4A**) and there are no significant difference of miR-27a(262 bp pri-miR-27a,78bp pre-miR27a, 22bp mature miR27a) between rLV-Cas9 group and rLV-Cas9–miR 24-2group (**FigureS4B**).These observations suggest that the knockout of t miR-24-2 did not affect the expression of miR-23a and miR-27a.

miR24-2 accelerates the growth of liver cancer stem cells *in vitro and in vivo.*

The positive rate of BrdU was significantly increased in the pCMV-miR24-2 group compared with the pCMV-miR group (19.46±2.27% vs 63.49±5.57%, P=0.00196) and reduced in the rLV-Cas9-miR24-2 group compared with the rLV-Cas9 group (23.12 ± 3.25% vs 7.01 ± 1.02%, P = 0.00777) (**Fig. S2D**).

Although there was no significant difference in the average scratch width at 0 hours of scratching among the pCMV-miR group, pCMV-miR24-2 group, rLV-Cas9 group, and rLV-Cas9-miR24-2 group (P>0.05), the average width ratio of scratches (24 hours/0 hours) after 24 hours of scratching was significantly reduced in the pCMV-miR24-2 group compared with the pCMV-miR group (0.0975±0.018 vs 0, P=0.0056) and increased the rLV-Cas9-miR24-2 group compared to the rLV-Cas9 group (0.0835 ± 0.0097 vs 0.2437 ± 0.0243, P = 0.00697 < 0.01) (**Fig. S2Ea&b**)

hLCSCs were infected with rLV-tet on-miR24-2, and the positive cells were picked up by several times under a fluorescence microscope, and were expanded. In stable hLCSCs cell lines , including DOX (0 μg/ml) group, DOX (0.5 μg/ml) group, DOX (1 μg/ml) group, DOX (2 μg/ml) group, precursor of miR24-2(pre-miR24-2) and the mature miR24-2 were significantly increased with increase of DOX concentration, and the pri-miR24-2 did not significantly change (**Fig. S2Ha-c**). The cell growth ability was significantly increased with the increase of DOX concentration (P<0.01) (**Fig.S2I**). The colony formation rate was significantly increased with the increase of DOX concentration (37.3±3.81% vs 56.63±5.42%, P=0.02109<0.05; 56.63 ±5.42% vs

70.15±3.02%, P=0.008446<0.01; 70.15±3.02% vs 87.21±7.41%, P=0.01327<0.05) (**Fig.S2J**). The sphere formation rate was significantly increased with the increase of DOX concentration, (15.08±3.45% vs 36.64±4.69%, P=0.00080848<0.01; 36.64±4.69% vs 55.30±5.33%, P=0.00074095<0.01; 55.30±5.33% vs 69.34±6.78%, P=0.0423375< 0.05) (**Fig.S2K**). The average weight of transplanted tumors in nude mice was significantly increased with the increase of DOX concentration (0.32±0.069 g vs 0.6±0.104 g, P=0.004451<0.01; 0.6±0.104).克 vs 0.82 ± 0.081 g, P = 0.0092314 < 0.01; 0.82 ± 0.081 g vs 1.31 ± 0.25 g, P = 0.0020429 < 0.01) **(Fig. S2La-b**). The average appearance time of transplanted tumor in nude mice was significantly decreased with the increase of DOX concentration (9.83±0.98 days vs 7.33±1.21 days, P=0.003374<0.01; 7.33 ± 1.21 days vs 5.67 ± 0.52 days, P = 0.00993 < 0.01; 5.67 ± 0.52 days vs 5.17 ± 0.75 days, P = 0.037779 < 0.05) (**Fig.S2Lc**). Collectively, these observations suggest that miR24-2 accelerates the growth of liver cancer stem cells *in vitro and in vivo.*

miR24-2 targets PRMT7 3 '-UTR and inhibits the expression of the PRMT7 in human liver cancer stem cells

In stable rLV-tet on-miR24-2 infected hLCSCs, including DOX (0 μg/ml) group, DOX (0.5 μg/ml) group, DOX (1μg/ml) group, DOX (2 μg/ml) group, pre-miR24-2 and the mature miR24-2 were significantly increased with increasing DOX concentration, and the pri-miR24-2 did not change significantly (**Fig. S5Ca-c**).Moreover, the binding ability of the mature miR24-2 or AgoII to PRMT7 3'-UTR was significantly increased with increasing DOX concentration (**Fig. S5D**) and the pEZX-MT-PRMT7 3'-UTR-Luc luciferase reporter gene activity were significantly decreased with increasing DOX concentration ($P<0.01$) (**Fig.S5E**). In addition, the pEZX-MT-PRMT7 3'-UTR (mutant)-Luc luciferase reporter gene activity did significantly not change with increasing DOX concentration **(Fig.S5F)**. Although there was no significant change in transcriptional level of PRMT7, the translational level of PRMT7 was significantly reduced as the increasing DOX concentration **(Fig.S5G)**. Taken together, these results suggest that miR24-2 targets PRMT7 3 '-UTR and inhibits the expression of the PRMT7 in human liver cancer stem cells.

miR24-2 affects the modification of trimethylation of arginine-3 of histone H4 on the HULC promoter region specifically

We performed the native CHIP with anti-H4R3me2 and anti-H4R3me3 to confirm the specific modification of dimethylation and trimethylation of arginine-3 of histone H4 on the HULC promoter region. We designed the CHIP primers according to the HULC promoter sequence[AL133261.8 (1..66219)](**FigureS6A**).

As shown in **FigureS6B**a, the modification of dimethylation of arginine-3 of histone H4 on the HULC promoter region of P7-P8 and P9-P10 was significantly decreased in rLV-miR24-2 group compared to rLV group and significantly increased in rLV-Cas9-miR24-2 group compared to rLV-Cas9 group. And the modification of dimethylation of arginine-3 of histone H4 on the HULC promoter region of P5-P6 and P11-P12 was not significantly altered in rLV group , rLV-miR24-2group ,rLV-Cas9 group and rLV-Cas9-miR24-2 group. And there was no the modification of dimethylation of arginine-3 of histone H4 on the HULC promoter region of P1-P2,P3-P4, P13-P14,P15-P16,P17-P18. Moreover, the real-time native CHIP obtained the similar findings(**FogureS6Bb**). Thus, miR24-2 affects the modification

of dimethylation of arginine-3 of histone H4 on the HULC promoter region of P7-P8 and P9-P10 specifically.

As shown in **FigureS6C**a, the modification of trimethylation of arginine-3 of histone H4 on the HULC promoter region of P7-P8 and P9-P10 was significantly decreased in rLV-miR24-2 group compared to rLV group and significantly increased in rLV-Cas9-miR24-2 group compared to rLV-Cas9 group. And the modification of trimethylation of arginine-3 of histone H4 on the HULC promoter region of P5-P6 , P11-P12 and P15-P16 was not significantly altered in rLV group , rLV-miR24-2group ,rLV-Cas9 group and rLV-Cas9-miR24-2 group. And there was no the modification of dimethylation of arginine-3 of histone H4 on the HULC promoter region of P1-P2,P3-P4, P13-P14,P17-P18. Moreover, the real-time native CHIP obtained the similar findings(**FogureS6Cb**). Thus, miR24-2 affects the modification of trimethylation of arginine-3 of histone H4 on the HULC promoter region of P7-P8 and P9-P10 specifically.

miR24-2 promotes the expression and maturation of miR675 via Nanog

In hLCSCs infected with rLV-tet on-miR24-2, both pre-miR24-2 and mature miR24-2 were increased significantly with increasing DOX concentration (**Fig.S7Aa&b**). In particular, the binding ability of Nanog, H3K9Ac and RNA polII to Pri-miR675 promoter cis-elements was significantly increased and the binding ability of HDAC4 to Pri-miR675 promoter cis-elements was significantly decreased with increasing DOX concentration,respectively(**Fig.S7B**).Moreover, the binding ability did significantly not change among rLV-tet on-miR24-2/DOX (0μg/ml) group, rLV-tet on-miR24-2/DOX(2μg/ml)+pGFP-V-RS-Nanog group (**Fig. S7C)**. And the binding capacity of RNApolII to pri-miR675 promoter cis-element probe was increased significantly as the increasing DOX concentration **(Fig. S7Da&b)**,and the binding capacity of RNApolII to the pri-miR675 promoter cis-element probe did significantly not change with increasing DOX concentration among rLV-tet on-miR24-2 /DOX (0μg/ml) group , rLV-tet on-miR24-2 /DOX (1 μg/ml) +pGFP-V-RS-Nanog group, rLV-tet on-miR24-2/DOX (2 μg/ml)+pGFP-V-RS-Nanog group **(Fig. S7Ea&b**). The pEZX-MT-Pri-miR675-Luc luciferase reporter gene activity was increased with increasing DOX concentration

(P<0.05 or P<0.01) (**Fig.S7F**). However, the luciferase reporter gene activity was significantly not changed with increasing DOX concentration among rLV-tet on-miR24-2 /DOX (0μg/ml) group, rLV-tet on-miR24-2/DOX(1μg/ml)+pGFP-V-RS-Nanog group, rLV-tet on-miR24-2/DOX (2μg/ml)+pGFP-V-RS-Nanog group (P>0.05)(**Fig.S7G**).

miR675 targets HDAC3 3'UTR and and inhibits translation of the *HDAC3* gene in human liver cancer stem cells

In hLCSCs infected with rLV, rLV-miR675, rLV-Cas9, and rLV-Cas9-miR675 respectively, the pre-miR675 and mature miR675 were increased in the rLV-miR675 group compared with the rLV group and knocked out in the rLV-Cas9-miR675 group compared with the rLV-Cas9 group (**FigureS8A&B**). Bioinformatics analysis revealed that the mature sequence of miR675 binds to the 3'-noncoding region (UTR) of histone deacetylase 3(HDAC3) mRNA through a 9-base seed sequence (**Fig. S8C**). pEZX-MT-HDAC3 3'-UTR-Luc reporter gene activity was significantly reduced in the rLV-miR675 group compared with the rLV group (P=0.003548<0.01) and significantly increased in the rLV-Cas9-miR675 group compared to rLV-Cas9 (P =

0.0005911< 0.01) (**Fig. S8D**). Although there was no significant change in the transcriptional level of HDAC3 in the rLV-miR675 group or rLV-Cas9-miR675 groups compared to the control group (**Fig. S8E**), the expression of HDAC3 was significantly reduced in the rLV-miR675 group compared to the rLV group and increased in the rLV-Cas9-miR675 group compared to the rLV-Cas9 group (**Fig. S8F)**. These results suggest that miR675 targets HDAC3 3'UTR and and inhibits translation of the *HDAC3* gene in human liver cancer stem cells

PI3K knockdown abrogates these actions of miR24-2 for autophagy

The expression of PI3K, LC3I and LC3II was significantly increased in the pCMV-miR24-2 group compared to the pCMV-miR group. However, there was no significant change between the pCMV-miR24-2+pGFP-V-RS-PI3K group and the pCMV-miR group(**Fig.S11A)**. The expression of PI3K, LC3I and LC3II were significantly increased in the DOX (2 μg/ml) group compared with the DOX (0 μg/ml) group. However, the expression of PI3K, LC3I and LC3II was significantly not changed in the rLV-tet on-miR24-2+pGFP-V-RS-PI3K/DOX (2μg/ml) group compared with the DOX (0 μg/ml) group (**Figure S11B**). The expression of LC3I and

LC3II was significantly increased in the DOX (2 μg/ml) group compared to the DOX (0 μg/ml) group. However, there was no significant change in rLV-tet on-miR24-2 + pGFP-V-RS-KAT8/DOX(2μg/ml) or rLV-tet on-miR24-2+pcDNA3-SET8 compared to the DOX (0 μg/ml) group (**Fig.S11C**). However, the interaction between the LC3 and ATG3 was not significantly changed in the pCMV-miR24-2+pGFP-V-RS-PI3K group compared to pCMV-miR group (**Fig. S11D**). The interaction between the LC3 and ATG3 was significantly increased in rLV-tet on-miR24-2/DOX (2μg/ml) group compared to the rLV-tet on-miR24-2/DOX (0 μg/ml) group. However, there was no significant change between rLV-tet on-miR24-2+pGFP-V-RS-PI3K/DOX (2μg/ml) group and the rLV-tet on-miR24-2/DOX (0 μg/ml) **(Fig.S11E)**. Moreover, the expression of the Beclin1 was significantly increased in the pCMV-miR24-2 group compared with the pCMV-miR group. However, the expression of the Beclin1 was not significantly changed between the pCMV-miR24-2+pGFP-V-RS-PI3K group and pCMV-miR group **(Fig.S11F).** The expression of Beclin1 was significantly increased in rLV-tet on-miR24-2/DOX (2μg/ml) group compared to the rLV-tet on-miR24-2/DOX (0 μg/ml) group . However, there was no significant change

between the rLV-tet on-miR24-2+pGFP-V-RS-PI3K/DOX (2 μg/ml) group and the rLV-tet on-miR24-2/DOX group(**Figure S11G**). The incidence of autophagy was significantly increased in the pCMV-miR24-2 group compared with the pCMV-miR group (10.39±1.76% vs 45.01±6.96%, P=0.008375<0.01). However, the incidence of autophagy was not significantly changed in the pCMV-miR24-2+pGFP-V-RS-PI3K group compared to pCMV-miR group (10.39±1.76% vs 5.93±2.29%, P=0.09818>0.05) **(Fig.S11Ha&b)**. The incidence of autophagy was significantly increased in rLV-tet on-miR24-2/DOX (2μg/ml) group compared to the rLV-tet on-miR24-2/DOX (0 μg/ml) group (5.58±3.01% vs 41.29±7.02%, P=0.00987011<0.01). However, there was no significant change between the rLV-tet on-miR24-2+pGFP-V-RS-PI3K/DOX (2 μg/ml) group and rLV-tet on-miR24-2/DOX(0 μg/ml) group (5.58±3.01% vs 6.85±1.67%, P=0.13632>0.05) **(Fig.S11Ia&b).** Collectively, these results suggest that miR24-2 promotes autophagy dependent on PI3K in human liver cancer stem cells.

Supplemental Figure legends

Figure S1 The isolation and identification of human liver cancer stem cell. **A.** the schematic diagram for isolating liver cancer stem cells from Huh7 liver cancer cell line using CD133/CD44/CD24/EpCAM microbeads (MicroBeads). B. The transcriptional ability of CD133, CD44, CD24, and Epcam was analyzed by reverse transcription polymerase chain reaction, and β-actin was used as an internal reference gene. C. Western blotting analysis using anti-CD133, anti-CD44, anti-CD24, anti-EpCAM, and β-actin as an internal reference gene. D. Comparison of human liver cancer stem cells (hLCSCs) and non-liver cancer stem cells (non-hLCSCs) isolated from human hepatoma cell Huh7 (bar ± SEM, n = 3), * *, $P < 0.01$, *, $P < 0.05$.

Figure S2 miR24-2 promotes growth of human liver cancer stem cells. A. The pCMV-miR or pCMV-miR24-2 were transfected into and the rLV-Cas9 or rLV-Cas9-miR24-2 were infected hLCSCs, respectively, and the positive cells were picked under fluorescent microscope and were expanded. The images taken with a fluorescence microscope (100×) was showed. B. The miR24-2 was detected by DOT-Blotting. U6 was used as an internal reference. C. Back-to-back RT-PCR was

used to detect the circular miR24-2. D. Determination of the S phase of hLCSCs cells by BrdU staining. a. BrdU stained photograph; b. Percentage of S phase cells. E. The wound test . a. Scratch photographs taken at 0 and 24 hours, respectively. b. Comparison of the average width of the scratches of the cells. F.4% formalin-fixed, paraffin-embedded nude mouse transplanted tumor tissue sections (4 μm) were subjected to hematoxylin-eosin (HE) (original magnification × 100). G. 4% formalin-fixed, paraffin-embedded nude mouse transplanted tumor tissue sections (4 μm) were subjected to the immunohistochemical staining of anti-PCNA (original magnification × 100). **H**. a. Northern-western blotting was used to detect the miR24-2.U6 serves as an internal reference. b. Dot blotting was used to detect the miR24-2. U6 serves as an internal reference. c. mature miR24-2 was detected by quantitative RT-PCR. U6 is used as an internal reference.**, $P < 0.01$, *, $P < 0.05$. I. The cell proliferation ability was determined by the CCK8. **, $P < 0.01$, *, $P < 0.05$. J. Plate colony formation ability was determined by crystal violet staining. K. The sphere formation ability of the cells.**, $P < 0.01$, *, $P < 0.05$. L. The hLCSCs were inoculated subcutaneously into Balb/C nude mice for 1 month. a. Photograph of

transplanted tumors (xenografts). b. Comparison of the size (g) of transplanted tumors in nude mice. c. Comparison of time (days) of transplanted tumors in nude mice (mean ± SEM, n = 6), **, $P < 0.01$, *, $P < 0.05$.

Figure S3 miR24-2 knockout identification. The DNA was isolated from hLCSCs stable infected with rLV-Cas9- miR24-2. The miR24-2 gRNA-intron fragment was analyzed by polymerase chain reaction, and β-actin was used as an internal reference gene. No band was shown if miR24-2 was knocked out. Positive miR24-2 knockout cell lines:2#,3#,6#,8#,11#,14#,15#,16#.

Figure S4 A. The Northern-Wstern blotting analysis of miR23a in rLV-Cas9 group and rLV-Cas9–miR24-2 group. **B.** The Northern-Western blotting analysis of miR27a in rLV-Cas9 group and rLV-Cas9–miR24-2 group

Figure S5 miR24-2 targets PRMT7 and inhibits HULC in human liver cancer stem cells. A. a. Northern-Western blotting was used to detect the miR24-2. U6 as an internal reference gene. b. Quantitative reverse transcription polymerase chain reaction (RT-PCR) was used to detect the miR24-2.U6 was used as an internal reference gene. B**.** The pEZX-MT-PRMT7 3'UTR(mutante)-Luc dual luciferase

reporter gene activity was tested. C.a. The miR24-2 was detected by Northern – Western blotting. U6 serves as an internal reference gene. b. Dot blotting was used to detect the miR24-2. GAPDH is used as an internal reference gene. c. The RT-PCR was performed to detect the mature miR24-2. U6 as an internal reference. D. The binding ability of the mature miR24-2, AgoII to PRMT7 3'-uncoding region (3'-UTR) was analyzed by RNA pulldown combined with RNA immunoprecipitation (RIP). E. The pEZX-MT-PRMT7 3'-UTR-Luc luciferase reporter gene activity was detected. F. The pEZX-MT-PRMT7 3'-UTR (mutant)-Luc luciferase reporter gene activity was detected . **, $P < 0.01$, *, $P < 0.05$. G. The PRMT7 was detected by RT-PCR and Western blotting. β-actin was used as an internal reference.

Figure S6 miR24-2 affects the modification of trimethylation of arginine-3 of histone H4 on the HULC promoter region specifically. A. the native CHIP primers were designed according to the HULC promoter sequence[AL133261.8 (1..66219)].

B .the modification of dimethylation of arginine-3 of histone H4 on the HULC promoter region was analyzed by native CHIP. C. B .the modification of

trimethylation of arginine-3 of histone H4 on the HULC promoter region was analyzed by native CHIP.

Figure S7 miR24-2 promotes expression and maturation of miR675 in stable human liver cancer stem cell lines (hLCSCs) infected with rLV-tet on-miR24-2 . A. rLV-tet on-miR24-2-infected stable human liver cancer stem cell lines (hLCSCs) were treated with different concentrations of DOX (0 μg/ml, 0.5 μg/ml, 1 μg/ml, 2 μg/ml), and then the total RNA was extracted. miR24-2 was detected by Northern blotting. U6 serves as an internal reference gene. b. mature miR24-2 was detected by quantitative reverse transcription polymerase chain reaction (RT-PCR). U6 is used as an internal reference gene. Each experiment was repeated three times. Each group of values is expressed as mean ± standard deviation (mean ± SEM, n = 3), **, $P < 0.01$, *, $P < 0.05$. B. Chromosome immunoprecipitation (CHIP) was performed using anti-Nanog, anti-HDAC4, anti-H3K9Ac, and anti-RNA polII. The polymer isolated and purified from the CHIP precipitate was used as a template, and polymerase chain reaction (PCR) amplification was carried out using a primer designed according to the Pri-miR675 promoter. IgG CHIP was used as a negative control; the DNA retained

before chromatin immunoprecipitation was used as a template, and the product amplified by the primer designed by the Pri-miR675 promoter was used as an internal reference (INPUT). C. Stable human hepatoma stem cell lines (hLCSCs) infected with rLV-tet on-miR24-2 (rLV-tet on-miR24-2 group) and rLV-tet on-miR24-2 infection + pGFP-V-RS-Nanog Transfected stable human hepatoma stem cell lines (hLCSCs) (rLV-tet on-miR24-2+pGFP-V-RS-Nanog group) were treated with different concentrations of DOX (1 μg/ml, 2 μg/ml). The binding ability of Nanog, HDAC4, H3K9Ac and RNA polII to the cis-miR675 promoter cis element was analyzed by chromatin immunoprecipitation (CHIP). D. a. The Super-DNA-protein complex gel Migration assay (Super-EMSA) using Biotin-labeled pri-miR675 promoter cis-element probe (Biotin-pri-miR675 promoter cis-element) and anti-RNA polII. Super-EMSA with IgG as a negative control, nucleoprotein-free EMSA and EMSA with excess cold probe as a system reference. b. Grayscale scan analysis of positive bands. E.a .The binding ability of RNApolII to the pri-miR675 promoter cis-element probe was analyzed using a Super-gel migration assay via biotin-labeled pri-miR675 promoter cis-element probe (Biotin-pri-miR675 promoter cis-element)

and anti-RNA polII, anti-Biotin. b. Grayscale scan analysis of positive bands. F. The stable human liver cancer stem cell lines (hLCSCs) infected with rLV-tet on-miR24-2 were treated with different concentrations of DOX (0 μg/ml, 0.5 μg/ml, 1 μg/ml, 1.5 μg/ml, 2 μg/ml).The pEZX-MT-Pri-miR675-Luc luciferase reporter gene plasmid carrying the pri-miR675 promoter was transfected into the above five stable liver cancer stem cell lines, and the activity of the luciferase reporter gene was detected 48 hours later. G. The stable human liver cancer stem cell lines (hLCSCs) infected with rLV-tet on-miR24-2 (rLV-tet on-miR24-2 group) and rLV-tet on-miR24-2 + pGFP-V-RS-Nanog were treated with different concentrations of DOX (0 μg/ml, 1 μg/ml, 2 μg/ml). The pEZX-MT-Pri miR675-Luc luciferase reporter plasmid carrying the pri-miR675 promoter was transfected into the above stable liver cancer stem cell lines, and the activity of the luciferase reporter gene was detected 48 hours later. Each experiment was repeated three times. Each group of values is expressed as mean ± standard deviation (mean ± SEM, n = 3), **, $P < 0.01$, *, $P < 0.05$.

Figure S8 miR675 targeted histone deacetylase HDAC3 in human liver cancer stem cell line. A. human liver cancer stem cell line (hLCSCs) was infected with

lentivirus rLV-miR675, lentivirus rLV, rLV-Cas9-miR675 and rLV-Cas9, respectively.Positive cells were screend and expanded. Then, total cellular RNA was extracted, and the miR675 in these four stable cell lines were detected by Northern blotting, U6 was used as an internal reference gene. **B.** Quantitative reverse transcription polymerase chain (RT-PCR) was used to detect the miR675 in these four stable cell lines, and U6 was used as an internal reference gene. **C.** Bioinformatics analysis of mature miR675 seed sequence binding to HDAC3 mRNA 3'-coding sequence (UTR) using MirTarget scanning soft software and BLAST tools. **D.** The pEZX-MT-HDAC3 3'-UTR-Luc luciferase reporter plasmid was transfected to the human liver cancer stem cell line hLCSCs and then the pEZX-MT-HDAC 3'-UTR-Luc dual luciferase reporter gene activity was detected. Each experiment was repeated three times. Each group of values is expressed as mean ± standard deviation (mean ± SEM, n = 3), **, $P < 0.01$, *, $P < 0.05$. **E**. Reverse transcription polymerase chain reaction (RT-PCR) was used to detect the transcriptional capacity of HDAC3 in these four stable cell lines, and β-actin was used as an internal reference gene. F.

Western blotting was used to detect the translational capacity of PRMT7 in these four stable cell lines, and β-actin was used as an internal reference gene.

FigureS9 miR24-2 enhances PI3K and affects autophagy in human liver cancer stem cells. A. chromosome immunoprecipitation(CHIP) with anti-H4K16Ac and anti-H3K20me2 were performed . B. The pGL4-PI3K-Luc luciferase reporter gene activity of the luciferase reporter gene was detected .**, $P < 0.01$, *, $P < 0.05$. C. The RT-PCR analysis was performed . β- actin serves as an internal reference gene. D. Western blotting with anti-PI3K was performed. β-actin as an internal reference gene. E. The RT-PCR was ued to detect PI3K . β-actin was used as an internal reference gene. F. Western blotting was performed using anti-PI3K. β-actin was used as an internal reference gene. **G**. The co-immunoprecipitation with anti-LC3 and the precipitate was analyzed by Western blotting with anti-ATG4.H. Western blotting was performed using anti-LC3.β-actin was used as an internal reference gene. I. The co-immunoprecipitation with anti-ATG3. J. Western blotting with anti-Beclin1. K. The infection of adenovirus rAd-Cherry-GFP-LC3 can monitor the autophagy through fluorescence microscopy directly. The occurrence of autophagy was observed (red

marker Cherry-LC3). L. a. Infection of adenovirus rAd-Cherry-GFP-LC3 can monitor the autophagy directly by fluorescence microscopy (red marker Cherry-LC3). b. Comparison of the incidence of autophagy. **, $P < 0.01$, *, $P < 0.05$.

Figure S10 miR24-2 affects expression. of PI3K dependent HDAC3-H4K16Ac-H4K20me2 in human liver cancer stem cells. A.a. The binding ability of H3K20me2 to the PI3K promoter cis-element probe was determined by Super-DNA-protein complex gel migration assay (Super-EMSA) using Biotin-labeled PI3K promoter cis-element probe (Biotin-PI3K promoter cis-element) and anti-H4K20me2, anti-Biotin. IgG super-EMSA was used as a negative control, EMSA without nucleoprotein and EMSA with excess cold probe were used as system reference, and the hybridization band of cis element of Biotin-PI3K promoter and the amount of nucleoprotein added were used as INPUT. b. Grayscale scan analysis of positive bands. B. a. The stable human liver cancer stem cell lines (hLCSCs) infected with rLV-tet on -miR24-2 and rLV-tet on-miR24-2+pcDNA3-HDAC3 were treated with different concentrations of DOX (0 μg/ml, 1 μg/ml, 2 μg/ml). The nuclear protein was extracted and the binding ability of RNApolII to the PI3K promoter

cis-element probe was determined by Super-gel migration. Super-DNA-protein complex gel migration assay (Super-EMSA) using Biotin-labeled PI3K promoter cis-element probe (Biotin-PI3K promoter cis-element) and anti-RNApolII, anti-Biotin IgG super-EMSA was used as a negative control, EMSA without nucleoprotein and EMSA with excess cold probe were used as system reference, and the hybridization band of cis element of Biotin-PI3K promoter and the amount of nucleoprotein added were used as INPUT. b. Grayscale scan analysis of positive bands. C. The pGL4-PI3K-Luc luciferase reporter gene plasmid was transfected into these stable liver cancer stem cell lines, and the activity of the luciferase reporter gene was detected 48 hours later. Each experiment was repeated three times. Each group of values is expressed as mean ± standard deviation (mean ± SEM, n = 3), **, $P < 0.01$, *, $P < 0.05$. D. The reverse transcription polymerase chain reaction (RT-PCR) using PI3K primers, and β-actin was used as an internal reference gene. E. The stable human liver cancer stem cell lines (hLCSCs) infected with rLV-tet on-miR24-2 + pGFP-V-RS-KAT8 , rLV-tet on-miR24-2 + pcDNA3-SET8 were treated with different concentrations of DOX (0μg/ml, 2μg/ml), and reverse transcription

polymerase chain reaction (RT-PCR) was performed using PI3K primers. β-actin as an internal reference gene. F. Western blotting with anti-PI3K, anti-KAT8, anti-SET8, anti-H4K16Ac and anti-H4K20me2, β-actin as internal Reference gene. G. Western blotting with anti-PI3K, anti-KAT8, anti-SET8, anti-H4K16Ac and anti-H4K20me2. β-actin is used as an internal reference gene.

Figure S11 miR24-2 increases autophagy dependent on phosphatidylinositol 3-kinase (PI3K) to in human liver cancer stem cells. A. The human livrer cancer stem cell lines (hLCSCs) transfected with pCMV-miR,pCMV-miR24-2 and pCMV-miR24-2+pGFP-V-RS-PI3K ,respectively, the total protein in the cell line was stabilized, and Western blotting was performed using anti-LC3 and anti-PI3K, and β-actin was used as an internal reference gene. B. Stable human liver cancer stem cell lines (hLCSCs) infected with rLV-tet on-miR24-2 and rLV-tet on-miR24-2 + pGFP-V-RS-PI3K, respectively, were treated with different concentrations of DOX (0 μg/ml, 2 μg/ml), and then total cellular proteins were extracted, and Western blotting was performed using anti-LC3 and anti-PI3K, and β-actin was used as an internal reference gene. C.The human liver cancer stem cell line infected with rLV-tet

on-miR24-2 and rLV-tet on -miR24-2 infection + pGFP-V-RS-KAT8 or pcDNA3-SET8 were treated with different concentrations of DOX (0 μg/ml, 2 μg/ml), and then total cellular proteins were extracted, western blotting was performed using anti-LC3, and β-actin was used as an internal reference gene. D. The experimental samples were co-immunoprecipitated with anti-ATG3, and the precipitates were analyzed by Western blotting with anti-LC3. IgG co-immunoprecipitation was used as a negative control, and the sample before coprecipitation was subjected to Western blotting with anti-ATG3 as INPUT. E. Stable human liver cancer stem cell lines (hLCSCs) infected with rLV-tet on-miR24-2 and rLV-tet on-miR24-2 infection + pGFP-V-RS-PI3K, respectively were treated with different concentrations of DOX (0 μg/ml, 2 μg/ml), then the total protein of the cells was extracted.The experimental samples were co-immunoprecipitated with anti-ATG3, and the precipitate was immunoblotted with anti-LC3. IgG co-immunoprecipitation was used as a negative control, and the sample before coprecipitation was subjected to Western blotting with anti-ATG3 as INPUT. F. human liver cancer stem cell lines (hLCSCs) transfected pCMV-miR pCMV-miR24-2 and pCMV-miR24-2+pGFP-V-RS-PI3K,respectively.

Western blotting was performed using anti-Beclin1, and β-actin was used as an internal reference gene. G. Stable human liver cancer stem cell lines (hLCSCs) infected with rLV-tet on-miR24-2 and rLV-tet on-miR24-2 infection+ pGFP-V-RS-PI3K were treated with different concentrations of DOX (0 μg/ml, 2 μg/ml) and then total cellular proteins were extracted.Western blotting was performed using anti-Beclin1, and β-actin was used as an internal reference gene. H. a. Human liver cancer stem cell lines (hLCSCs) transfected with pCMV-miR , pCMV-miR24-2, and pCMV-miR24-2+pGFP-V-RS-PI3K ,respectively. The infection of the adenovirus rAd-Cherry-GFP-LC3 was able to monitor the autophagy directly by fluorescence microscopy (red marker Cherry-LC3). b. Comparison of the incidence of autophagy in cells. Each experiment was repeated three times. Each group of values is expressed as mean ± standard deviation (mean ± SEM, n = 3), **, $P < 0.01$, *, $P < 0.05$. I.a .human liver cancer stem cell lines (hLCSCs) infected with rLV-tet on-miR24-2 and rLV-tet on-miR24-2 + pGFP-V-RS-PI3K,respectively were treated with the concentration of DOX (0μg/ml, 2μg/ml).The adenovirus rAd-Cherry-GFP-LC3, which can monitor autophagy, was directly infected, and then

the autophagy occurred after cell starvation was directly observed by fluorescence microscope (red marker Cherry-LC3). b. Comparison of the incidence of autophagy in cells. Each experiment was repeated three times. Each group of values is expressed as mean ± standard deviation (mean ± SEM, n = 3), **, $P < 0.01$, *, $P < 0.05$.

Figure S12 4% formaldehyde-fixed, paraffin-embedded transplanted tumor tissue section (4 μm) was subjected to hematoxylin-eosin (HE) (original magnification × 100).

Figure S13 The molecular mechanism that miR24-2 promotes malignant growth of liver cancer stem cells. miR24-2 enhances the expression and function of the tyrosine protein kinase sarcoma gene Src in liver cancer stem cells and promotes the malignant growth of liver cancer stem cells. First, the mature sequence of miR24-2 binds to the protein arginine methyltransferase 7 (PRMT7) mRNA 3' noncoding region (UTR) and thus inhibits the translational ability of the *PRMT7* gene. Then, miR24-2 inhibited the bi- (tri)methylation of histone 4 arginine by reducing

PRMT7 (H4R3me2 and H4R3me3), significantly reducing the binding capacity of H4R3me2 and H4R3me3 to HULC promoter, promoting HULC expression. miR24-2-dependent HULC promoted the binding of C-myc, Epcam and KLF4 to the Nanog promoter in human hepatoma stem cells, and promoted its transcriptional activity and expression. Moreover, miR24-2 inhibits the expression of histone deacetylase HDAC3 in human hepatoma stem cells through miR675, and promotes the acetylation of lysine at position 16 of Histone H4 in human liver stem cells, and relies on the 16th lysine of Histone H4. The acetylation modification of the acid inhibits the methylation modification of the 20th lysine of Histone H4. Moreover, miR24-2 increased histone H4K16Ac and attenuated the binding ability of H4K20me2 to enhance expression of PI3K. Subsequently, miR24-2 is dependent on PI3K to enhance the expression of autophagy structural protein LC3 and its interaction with the cleavage protein ATG4. Thereby, LC3 is further matured into activated LC3II, and the interaction between LC3II and processing protein ATG3. Then miR24-2 enhances the interaction between PKM1 and autophagosome functional protein P62, and enhances the protection of PKM1 by autophagy of liver

cancer stem cells, and inhibits the degradation of PKM1.Interestingly, miR24-2 promotes the binding of PKM1 to the tyrosine protein kinase sarcoma gene Src promoter and enhances the the expression of *Src*. Moreover, the *Src* gene plays an important role in the malignant growth of human liver cancer stem cells triggered by miR24-2.

Supplemental Figure

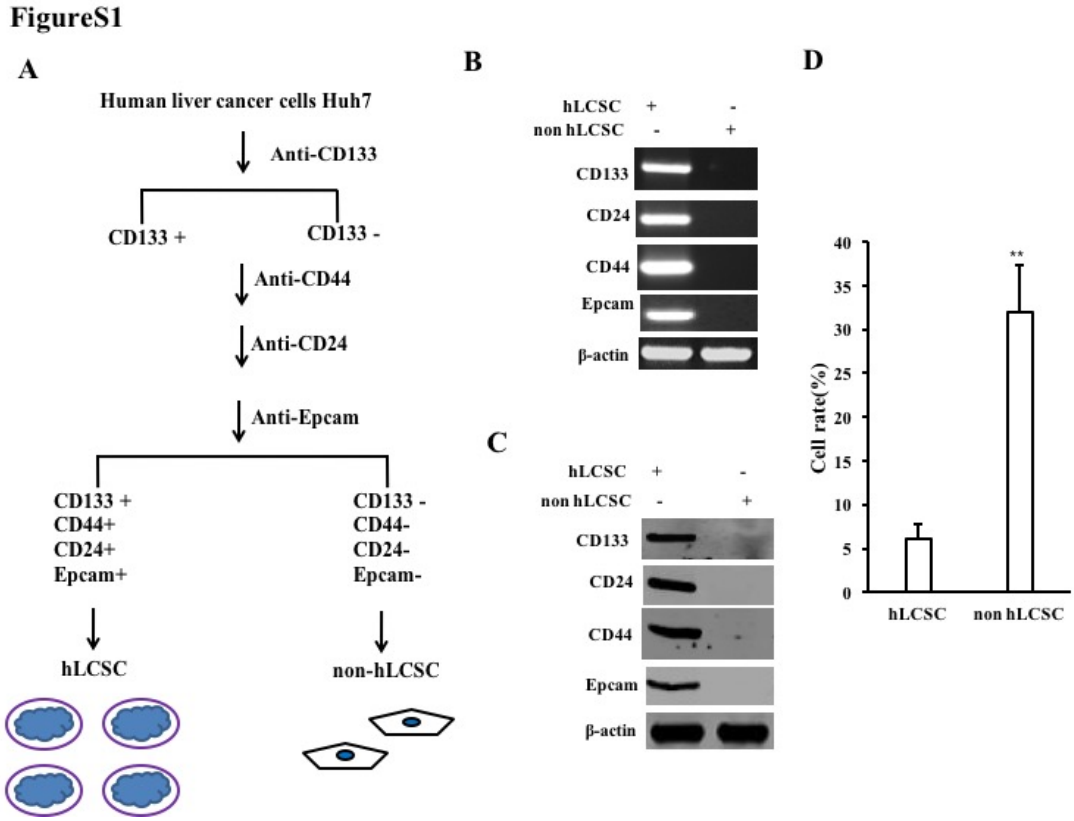

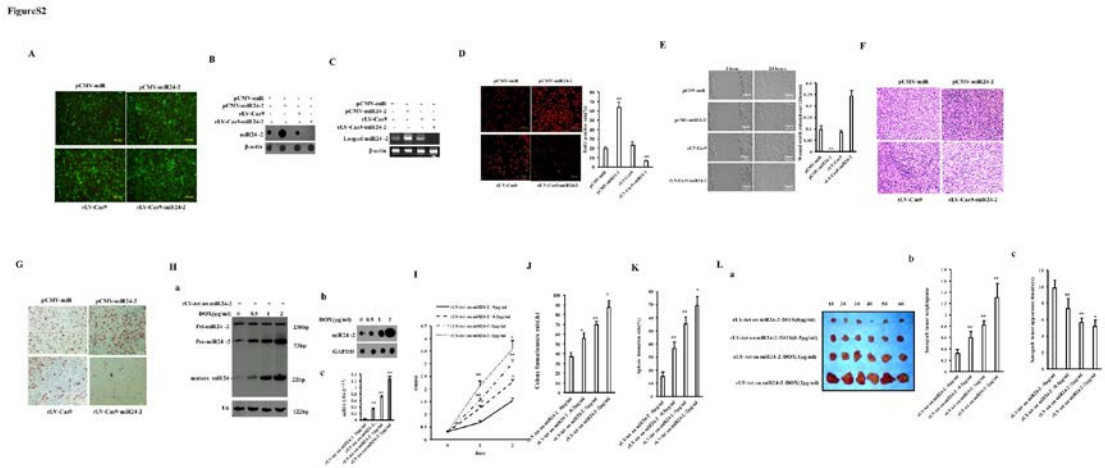

FigureS3

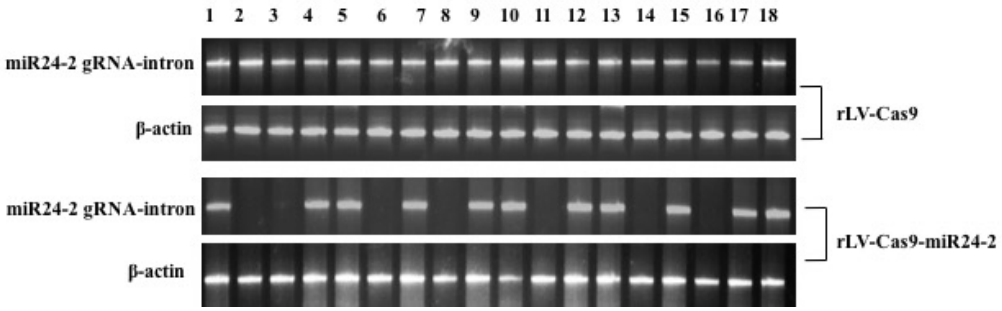

FigureS4

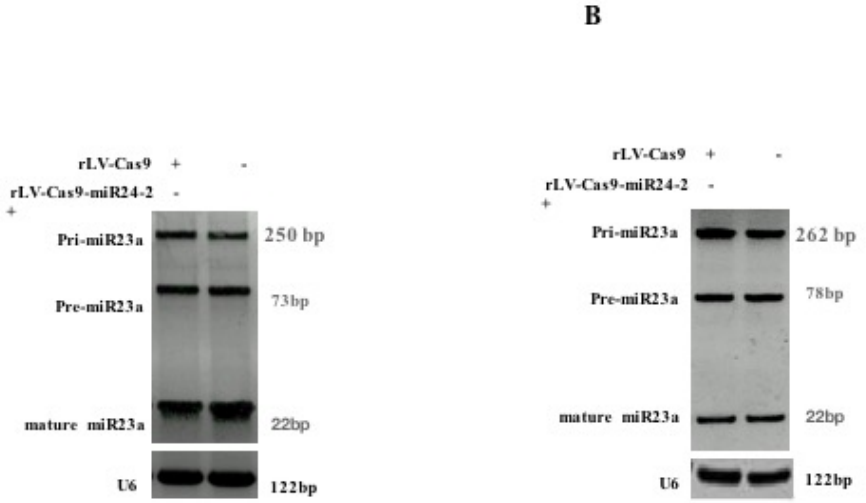

Figure S5

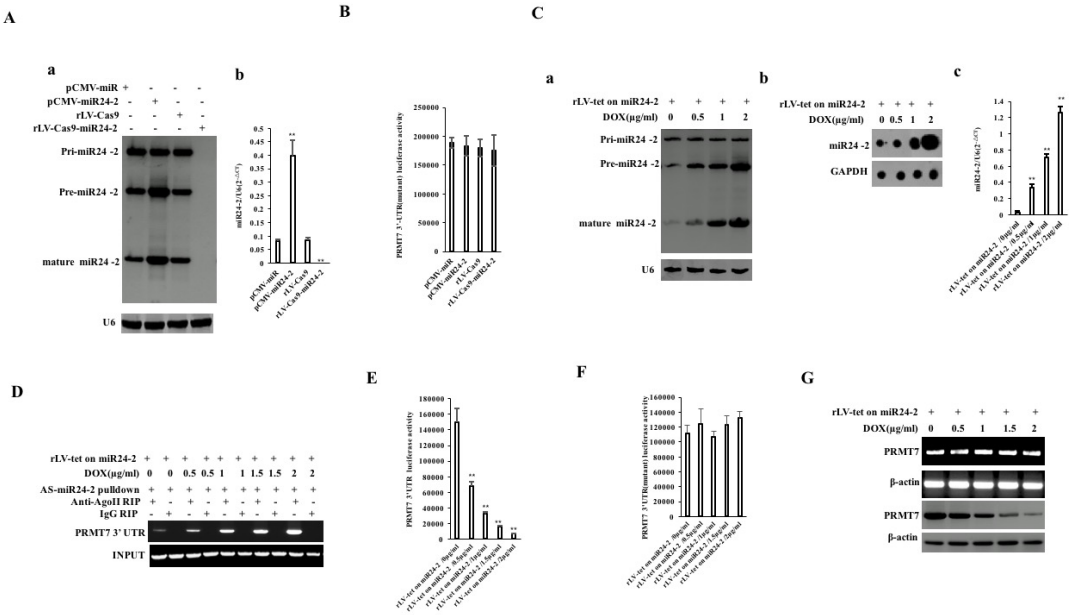

FigureS6

A

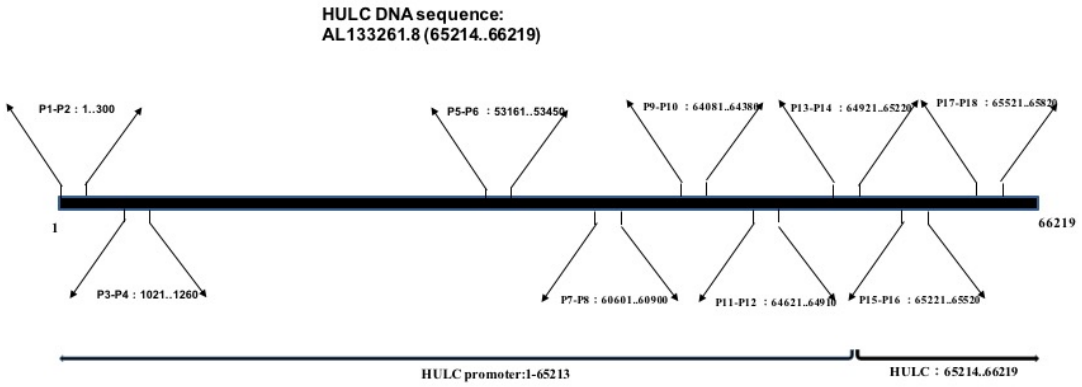

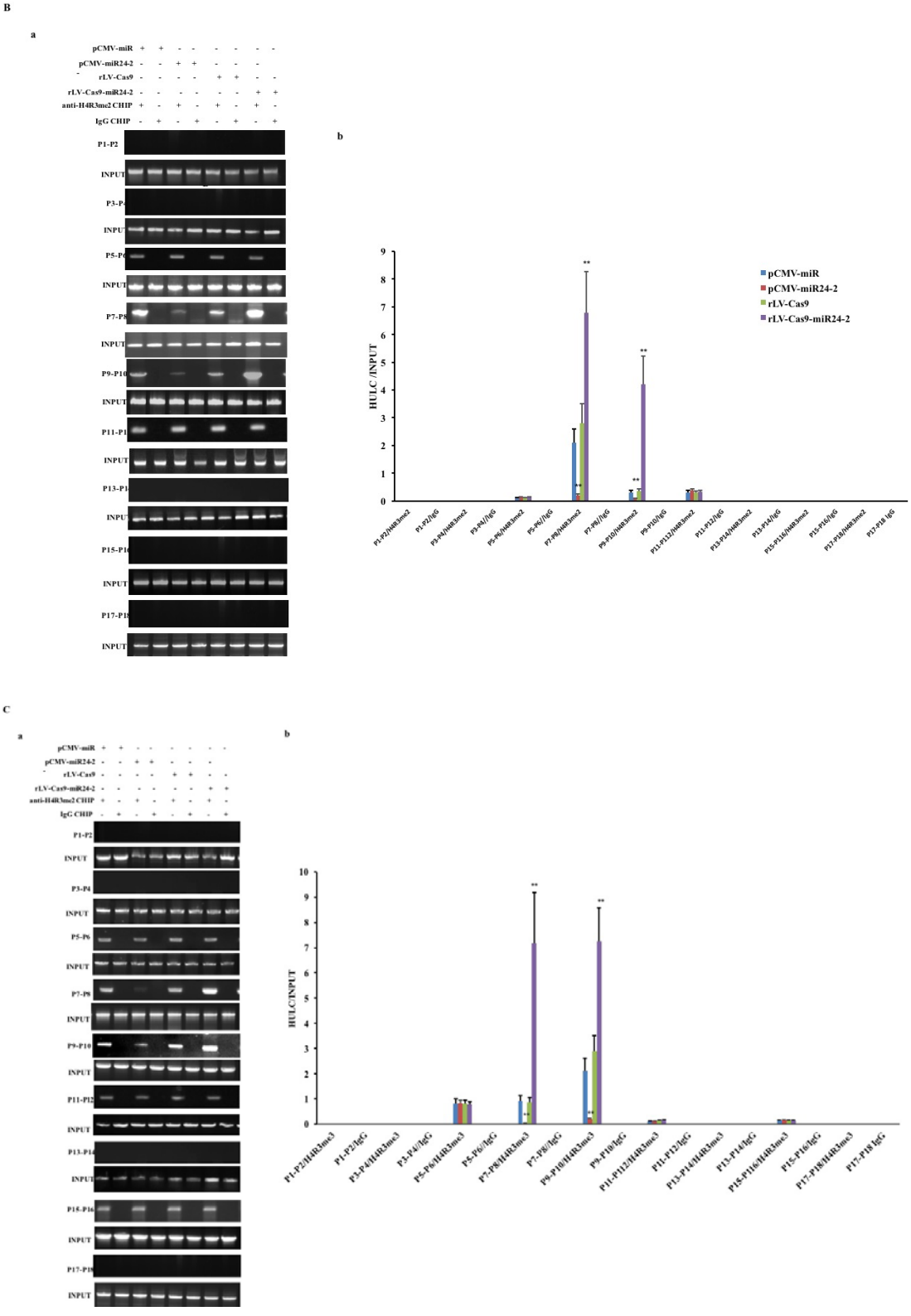
B
a
pCMV-miR
pCMV-miR24-2
rLV-Cas9
rLV-Cas9-miR24-2
anti-H4R3me2 CHIP
IgG CHIP
P1-P2
INPUT
P3-P4
INPUT
P5-P6
INPUT
P7-P8
INPUT
P9-P10
INPUT
P11-P12
INPUT
P13-P14
INPUT
P15-P16
INPUT
P17-P18
INPUT
b
HULC /INPUT
pCMV-miR
pCMV-miR24-2
rLV-Cas9
rLV-Cas9-miR24-2
P1-P2/H4R3me2
P1-P2/IgG
P3-P4/H4R3me2
P3-P4/IgG
P5-P6/H4R3me2
P5-P6//IgG
P7-P8/H4R3me2
P7-P8//IgG
P9-P10/H4R3me2
P9-P10/IgG
P11-P12/H4R3me2
P11-P12/IgG
P13-P14/H4R3me2
P13-P14/IgG
P15-P116/H4R3me2
P15-P16/IgG
P17-P18/H4R3me2
P17-P18 IgG
C
a
pCMV-miR
pCMV-miR24-2
rLV-Cas9
rLV-Cas9-miR24-2
anti-H4R3me2 CHIP
IgG CHIP
P1-P2
INPUT
P3-P4
INPUT
P5-P6
INPUT
P7-P8
INPUT
P9-P10
INPUT
P11-P12
INPUT
P13-P14
INPUT
P15-P16
INPUT
P17-P18
INPUT
b
HULC/INPUT
P1-P2/H4R3me3
P1-P2/IgG
P3-P4/H4R3me3
P3-P4/IgG
P5-P6/H4R3me3
P5-P6//IgG
P7-P8/H4R3me3
P7-P8//IgG
P9-P10/H4R3me3
P9-P10/IgG
P11-P12/H4R3me3
P11-P12/IgG
P13-P14/H4R3me3
P13-P14/IgG
P15-P116/H4R3me3
P15-P16/IgG
P17-P18/H4R3me3
P17-P18 IgG

FigureS7

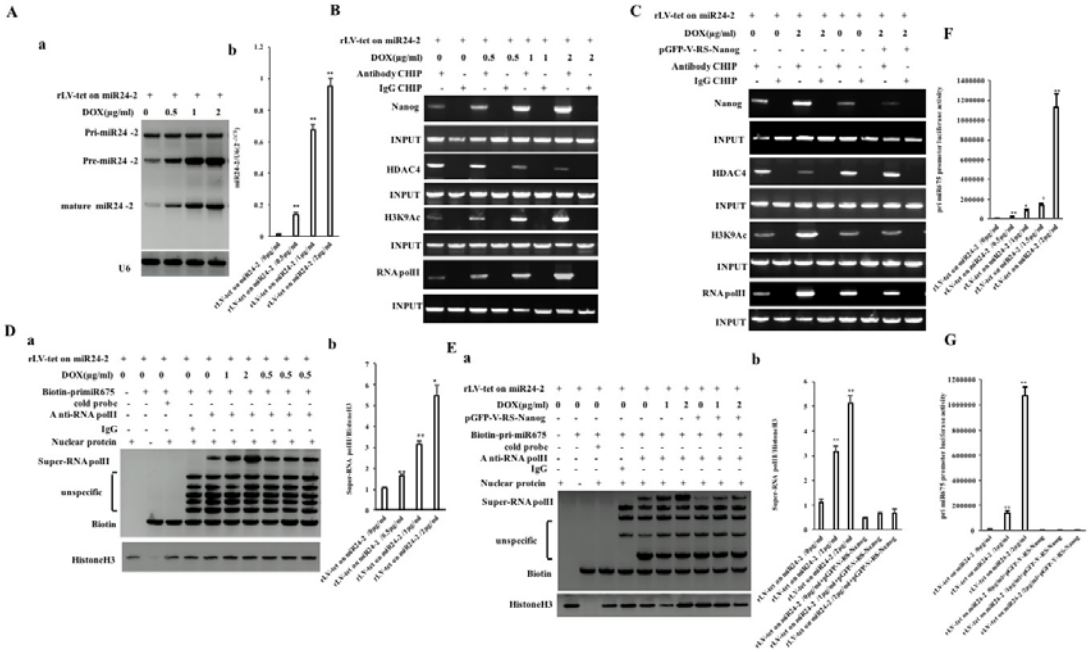

FigureS8

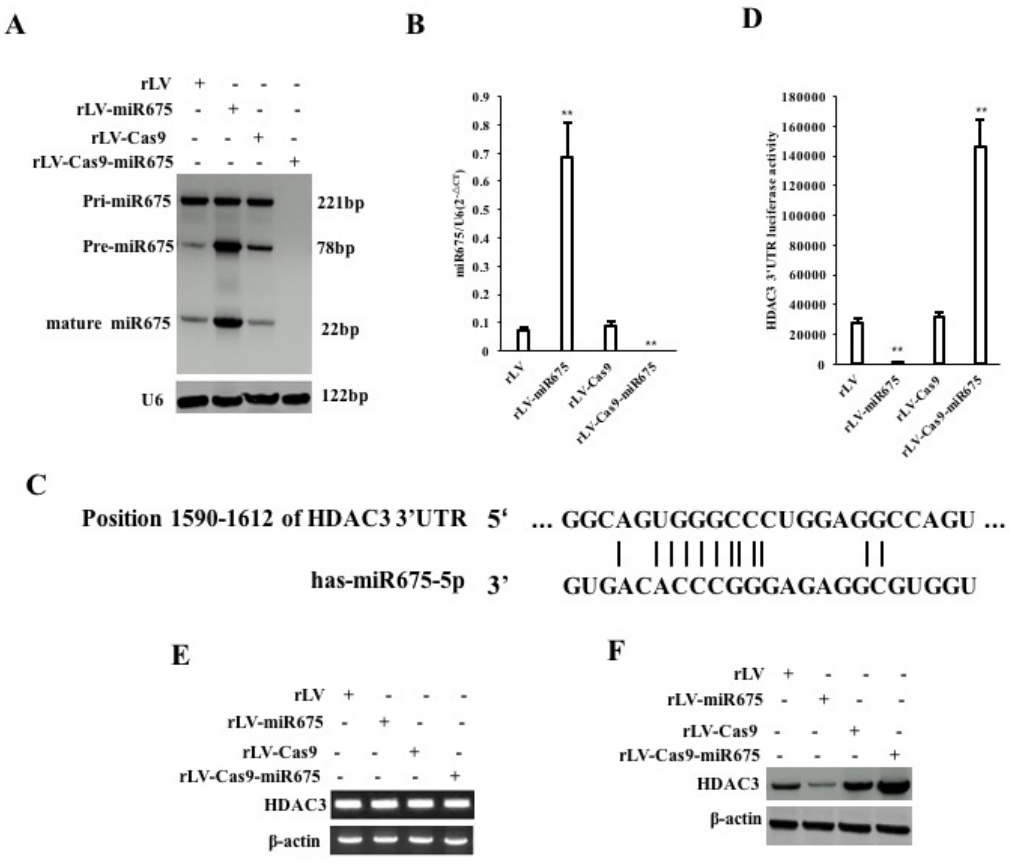

FigureS9

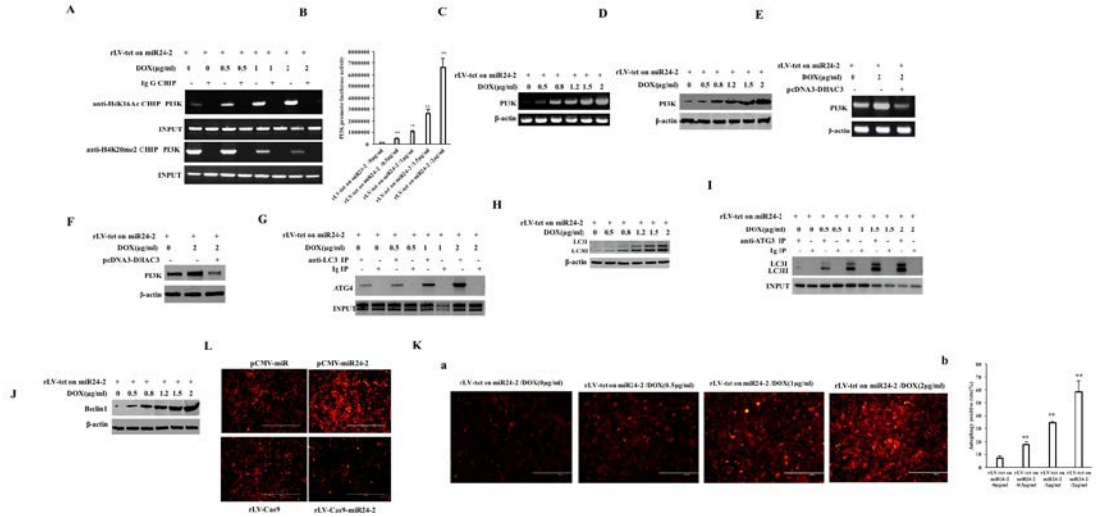

FigureS10

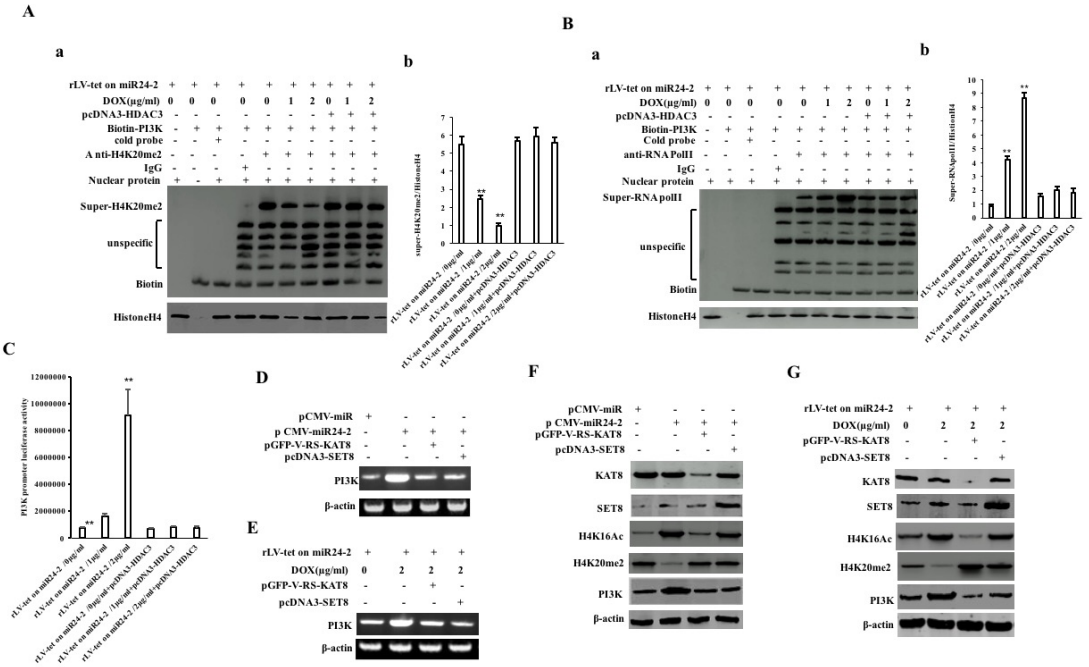

FigureS11

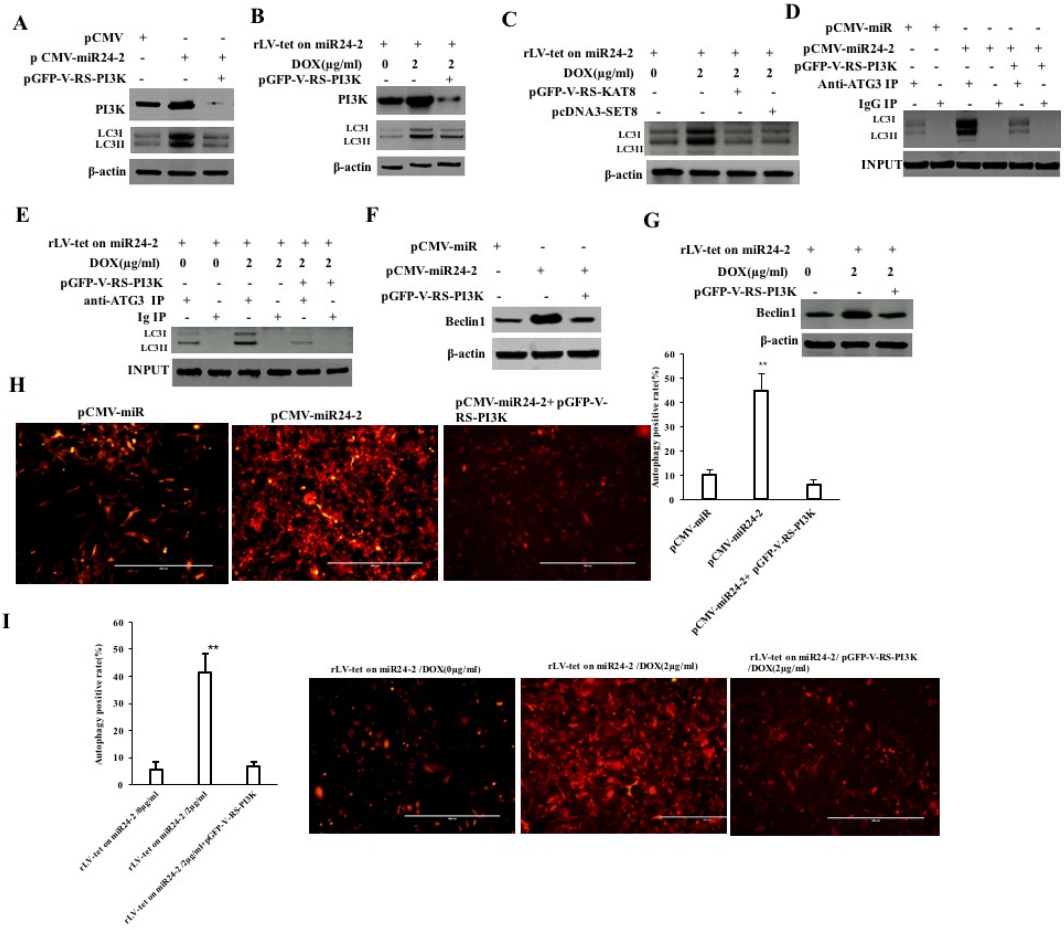

FigureS12

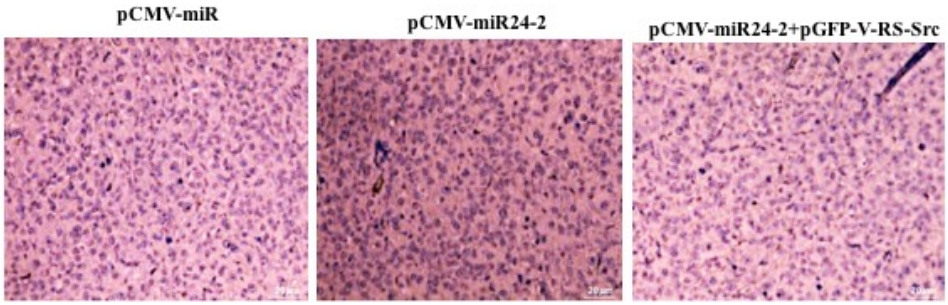

FigureS13

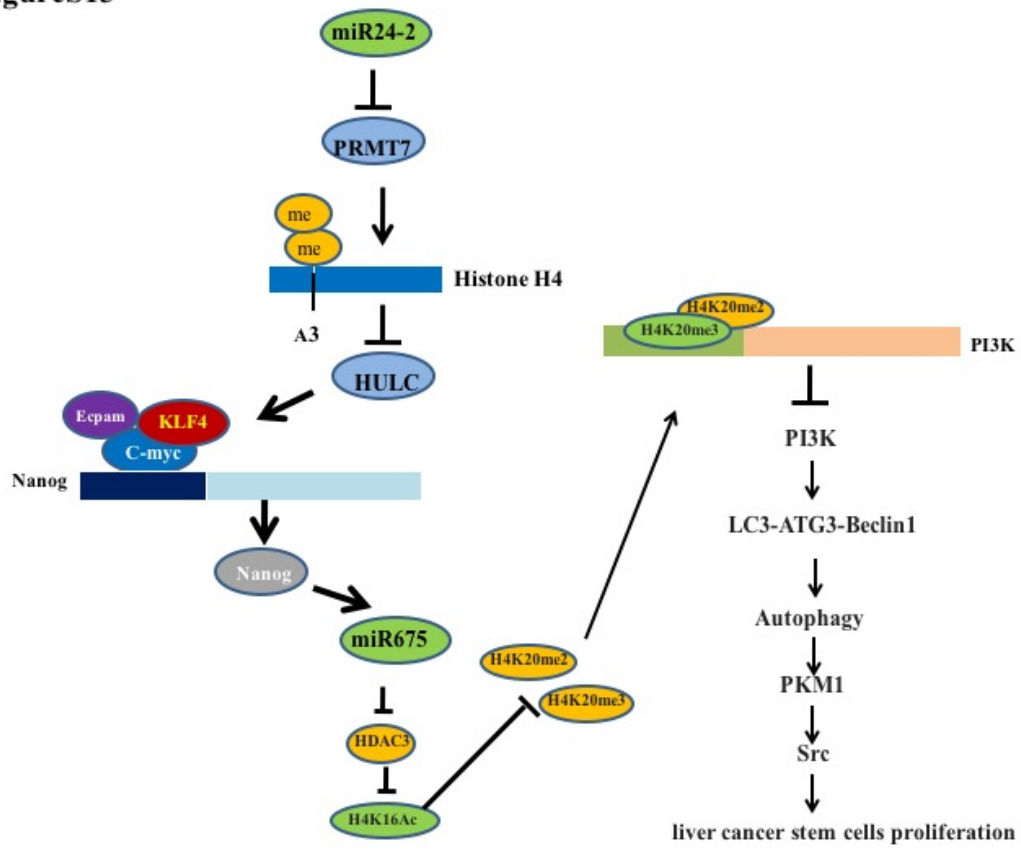
miR24-2
PRMT7
me
me
Histone H4
A3
HULC
Ecpam
KLF4
C-myc
Nanog
Nanog
miR675
HDAC3
H4K16Ac
H4K20me2
H4K20me3
H4K20me2
H4K20me3
PI3K
PI3K
LC3-ATG3-Beclin1
Autophagy
PKM1
Src
liver cancer stem cells proliferation